Neurobiology of Disease 194 (2024) 106474

Contents lists available at ScienceDirect

Neurobiology of Disease

journal homepage: www.elsevier.com/locate/ynbdi

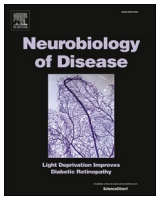

Engrailed 1 deficiency induces changes in ciliogenesis during human neuronal differentiation

Sina Hembach [a,b,1], Sebastian Schmidt [a,c,d,1], Tanja Orschmann [a], Ingo Burtscher [e], Heiko Lickert [e,f,g], Florian Giesert [a], Daniela Vogt Weisenhorn [a], Wolfgang Wurst [a,d,h,i,j,*]

[a] Institute of Developmental Genetics, Helmholtz Munich, Neuherberg, Germany
[b] Munich School of Life Sciences Weihenstephan, Technical University of Munich, Munich, Germany
[c] Neurobiological Engineering, Munich Institute of Biomedical Engineering, TUM School of Natural Sciences, Garching, Germany
[d] Deutsche Zentrum für Psychische Gesundheit (DZPG), Site Munich-Augsburg, Munich, Germany
[e] Institute of Diabetes and Regeneration Research, Helmholtz Munich, Neuherberg, Germany
[f] German Center for Diabetes Research (DZD), Neuherberg, Germany
[g] School of Medicine, Technische Universität München, Munich, Germany
[h] Technische Universität München-Weihenstephan, Neuherberg, Germany
[i] Munich Cluster for Systems Neurology (SyNergy), Munich, Germany
[j] German Center for Neurodegenerative Diseases (DZNE) Munich, Munich, Germany

ARTICLE INFO

Keywords:
Engrailed 1
dopaminergic neuron
primary cilia
Wnt signaling
induced pluripotent stem cells
complex I
mitochondrial respiration

ABSTRACT

A key pathological feature of Parkinson's Disease (PD) is the progressive degeneration of dopaminergic neurons (DAns) in the substantia nigra pars compacta. Considering the major role of EN1 in the development and maintenance of these DAns and the implications from En1 mouse models, it is highly interesting to study the molecular and protective effect of EN1 also in a human cellular model. Therefore, we generated *EN1* knock-out (ko) human induced pluripotent stem cell (hiPSCs) lines and analyzed these during neuronal differentiation. Although the *EN1* ko didn't interfere with neuronal differentiation and generation of tyrosine hydroxylase positive (TH+) neurons per se, the neurons exhibited shorter neurites. Furthermore, mitochondrial respiration, as well as mitochondrial complex I abundance was significantly reduced in fully differentiated neurons. To understand the implications of an *EN1* ko during differentiation, we performed a transcriptome analysis of human neuronal precursor cells (hNPCs) which unveiled alterations in cilia-associated pathways. Further analysis of ciliary morphology revealed an elongation of primary cilia in *EN1*-deficient hNPCs. Besides, also Wnt signaling pathways were severely affected. Upon stimulating hNPCs with Wnt which drastically increased *EN1* expression in WT lines, the phenotypes concerning mitochondrial function and cilia were exacerbated in *EN1* ko hNPCs. They failed to enhance the expression of the complex I subunits NDUFS1 and 3, and now displayed a reduced mitochondrial respiration. Furthermore, Wnt stimulation decreased ciliogenesis in *EN1* ko hNPCs but increased ciliary length even further. This further highlights the relevance of primary cilia next to mitochondria for the functionality and correct maintenance of human DAns and provides new possibilities to establish neuroprotective therapies for PD.

1. Introduction

Parkinson's Disease (PD) is a progressive neurodegenerative disorder that affects the dopaminergic population in the substantia nigra pars compacta (SNpc). The degeneration of these neurons is associated with characteristic motor symptoms like bradykinesia, resting tremor, and rigidity (Poewe et al., 2017). Although the underlying causes remain elusive, multiple molecular mechanisms are thought to contribute to the etiology of PD including oxidative stress, and a mitochondrial complex I deficiency, next to other mitochondrial dysfunctions (Giguère et al., 2018; Poewe et al., 2017; Schmidt et al., 2022a; Surmeier et al., 2017).

EN1 is an interesting candidate to be investigated in the context of

* Corresponding author.
E-mail address: wolfgang.wurst@helmholtz-munich.de (W. Wurst).
[1] Authors contributed equally

https://doi.org/10.1016/j.nbd.2024.106474
Received 23 January 2024; Received in revised form 15 March 2024; Accepted 15 March 2024
Available online 20 March 2024

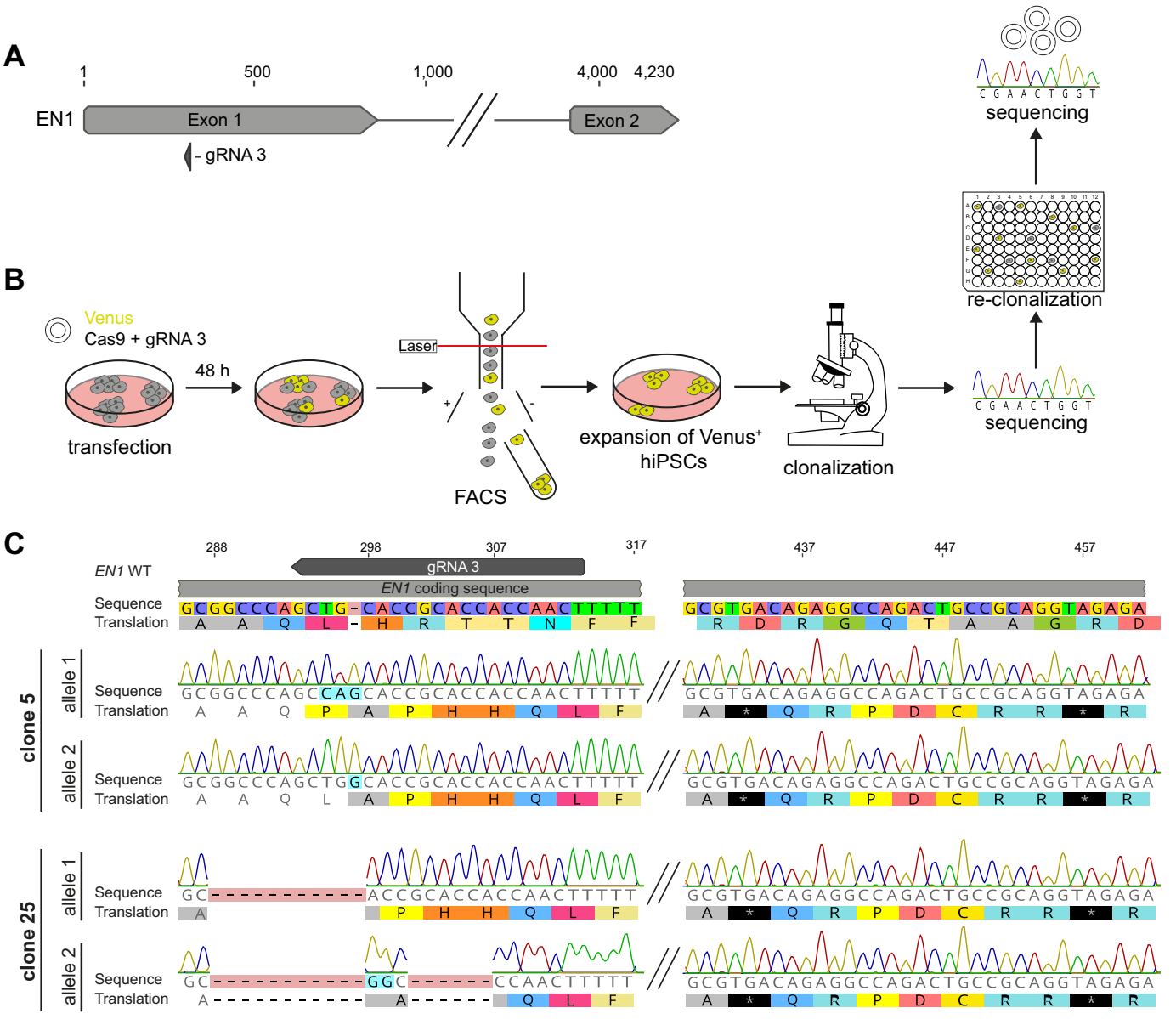

Fig. 1. Targeting strategy, workflow, and sequence of *EN1* knock-out clones.
(A) Binding site of the gRNA within the *EN1* coding sequence.
(B) Workflow for the generation of the *EN1* knock-out hiPSCs and corresponding WT control clones. Transfected cells were sorted and clonalized twice.
(C) Sequences show the CRISPR/Cas9 induced nucleotide alterations after subcloning of the respective mRNA for both alleles as well as the amino acid sequences for *EN1* ko clones. The gRNA target region and the nucleotide positions from the transcription start site are indicated at the top.

PD, as it is essential for the development as well as the post-mitotic survival of midbrain dopaminergic neurons (DAns) (Alavian et al., 2014). *En1* expression starts at embryonic day 8 (E8) in mice and is responsible for correct mid-hindbrain patterning during development (Liu and Joyner, 2001). At this point, the expression of *En1* is maintained by *Wnt1* which mediates Tcf/Lef binding to the *En1* promotor (Danielian and McMahon, 1996; Davis and Joyner, 1988; Kim et al., 2018; McGrew et al., 1999). From E11 onwards, *En1* is expressed in DAns where it is crucial for neuronal survival in a dose-dependent and cell-autonomous manner (Albéri et al., 2004; Simon et al., 2001). The importance of En1 for the survival of DAns has been strengthened by observations from *En1* knock-out (ko) mouse models. Whereas homozygous *En1* ko's die within 24 h after birth (Wurst et al., 1994), the heterozygous *En1* ko is viable with a normal number of dopaminergic neurons at birth. However, starting at the age of 8 weeks, the DAns degenerate progressively which recapitulates one of the major pathological hallmarks of PD. As PD patients, the animals display retrograde degeneration of the nigrostriatal neurons which results in impaired motor skills including abnormal spontaneous motor behavior, deficits in motor coordination, as well as in non-motor symptoms like enhanced resignation and anhedonic-like behavior (Sgadò et al., 2006; Sonnier et al., 2007). The loss of DAns in heterozygous *En1* mice was not evident when Wnt1 was expressed under the *En1* promotor ($En1^{+/Wnt1}$), which supports the hypothesis that Wnt1 is an upstream regulator of *En1* expression (Zhang et al., 2015).

En1 is also linked to mitochondrial function, more specifically to complex I activity. Enhanced translation of the two complex I subunits NADH:Ubiquinone oxidoreductase core subunit S1 (Ndufs1) and NADH: Ubiquinone oxidoreductase core subunit S3 (Ndufs3) have been associated with the neuroprotective effect of En1 in a 1-methyl-4-phenyl-1,2,3,6-tetrahydropyridine (MPTP) Parkinson's disease mouse model. Besides, reduced levels of Ndufs1 and Ndufs3 have been found in the

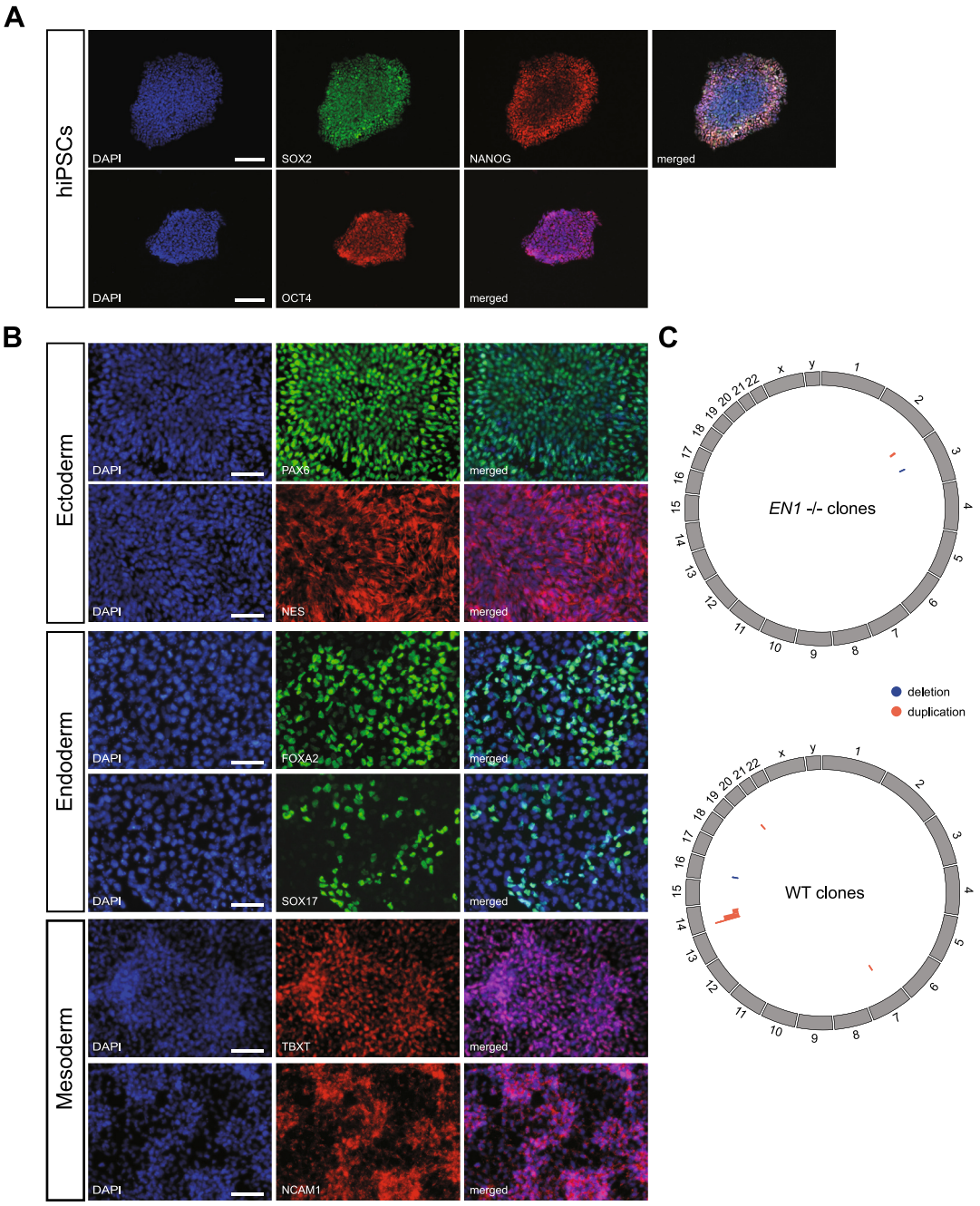

Fig. 2. Quality control of generated hiPSCs.
(A) Immunofluorescence staining of hiPSCs for the pluripotency markers SOX2, NANOG, and OCT4 shown exemplarily for *EN1* ko clone 25-19. Scale bars: 200 µm.
(B) Immunofluorescence staining for ectodermal (PAX6, NESTIN), endodermal (FOXA2, SOX17), and mesodermal (TBTX, NCAM1) markers after tri-lineage differentiation of hiPSCs shown exemplarily for *EN1* ko clone 5-12. Scale bars: 100 µm.
(C) Circos plots show the distribution of somatic CNVs for *EN1* ko and WT clones.

SNpc of heterozygous *En1* ko mice (Alvarez-Fischer et al., 2011). It has already been shown that En1, in addition to its role as a transcription factor, also regulates mRNA translation. This process has first been shown in growth cones and is mediated through the mTOR pathway and binding to the eukaryotic translation initiation factor 4E (eIF4E) (Alvarez-Fischer et al., 2011; Brunet et al., 2005). This further highlights a possible involvement of En1 in PD etiology, as varying degrees of complex I deficiency have also been described in postmortem brain tissue of PD patients or human induced pluripotent stem cell (hiPSC)-derived models of sporadic PD (Schmidt et al., 2022a).

Considering the major role of En1 in the development and maintenance of DAns in mice, it is important to obtain reliable data on EN1 function in humans. Such data are warranted to elucidate its possible therapeutic potential in PD. Therefore, we generated *EN1* ko hiPSC lines and differentiated these hiPSCs into the dopaminergic lineage. The neuronal cells were assessed regarding their differentiation potential into TH+-neurons and their mitochondrial functionality. A transcriptome analysis of neuronal precursor cells (hNPCs) as an intermediate stage during neuronal differentiation, allowed us to identify dysregulated genes that are associated with primary cilia (PC) function and signal transduction. A cellular analysis revealed impairments in PC morphology. These alterations were even enhanced upon stimulating the Wnt signaling pathway, which depends on functional PC and induces a massive upregulation of EN1. Additionally, the *EN1* ko hNPCs failed to

Table 1
Overview of the selected *EN1* ko, and WT clones. The nucleotide alterations and the effect on protein translation are listed. Shaded clones were excluded after quality control.

Clone	Subclone	Genotype	Mutation	Protein sequence
5	5-6	*EN1 ko*	1 bp insertion 1bp insertion and 1 bp mutation	Frameshift and premature stop codons at nucleotide positions 432 and 456
	5-12	*EN1 ko*	1 bp insertion 1bp insertion and 1 bp mutation	Frameshift and premature stop codons at nucleotide positions 432 and 456
25	25-16	*EN1 ko*	11 bp deletion 17 bp deletion	Frameshift and premature stop codons at nucleotide positions 432 and 456
	25-19	*EN1 ko*	11 bp deletion 17 bp deletion	Frameshift and premature stop codons at nucleotide positions 432 and 456
WT 4	4-3	WT	none	WT
	4-4	WT	none	WT
	4-5	WT	none	WT
WT 11	11-2	WT	none	WT
WT 15	15-1	WT	none	WT
WT 18	18-3	WT	none	WT

enhance the expression of the complex I subunits NDUFS1 and 3 upon Wnt stimulation and now displayed reduced mitochondrial respiration. These results highlight the influence of EN1 on Wnt signal transduction and identify PC alongside mitochondria as an essential factor that is cooperatively maintained by EN1 and Wnt during neuronal differentiation and survival.

2. Results

2.1. Generation of an EN1 knock-out human model system

To investigate the function of *Engrailed 1* (*EN1*) on a human background, *EN1* knock-out (ko) hiPSCs were generated using CRISPR/Cas9. DNA double-strand breaks were induced at the beginning of exon 1 using a single gRNA targeting approach (Fig. 1A). Following transfection with a plasmid encoding for Cas9, the gRNA, and a Venus reporter, the reporter-positive cells were selected by FACS. Clones harboring mutations in the *EN1* locus that resulted in a frameshift and premature termination of translation were selected and clonalized to ensure a homogeneous genotype (Fig. 1B). Only clones with two different mutations leading to the formation of a biallelic ko were selected. Two clones exhibited biallelic mutations that generated premature stop codons at nucleotide positions 432 or 456 base pair (bp) downstream of the transcription start site, respectively (Fig. 1C). Clone 5 had an insertion of 1 bp on one allele and a 1 bp insertion combined with a single nucleotide polymorphism (SNP) on the other allele. Clone 25 possessed an 11 bp deletion and a 17 bp deletion, respectively. To also account for hiPSC variability (Volpato and Webber, 2020), multiple subclones were selected for further experiments. Isogenic WT control clones were generated in parallel by subjecting untargeted hiPSCs to the same two-step clonalization procedure as described above (Fig. 1B).

Following the generation of the *EN1* ko, hiPSCs were subjected to thorough quality control to ensure genomic integrity and pluripotency. All selected *EN1* ko and WT clones showed normal colony-forming morphology and expressed the pluripotency markers OCT4, SOX2, and NANOG (Fig. 2A). In addition, all clones showed pluripotent characteristics by differentiating into the three germ layers as assessed by trilineage differentiation and immunostaining for ectodermal, endodermal, and mesodermal markers, respectively (Fig. 2B). The clones were further screened for copy number variations (CNVs) using an SNP microarray to ensure genomic integrity (Fig. 2C) (Table 1; Table S1). The ko clones showed no CNVs except for subclone 25-16, which exhibited a duplication of about 5,400 kilo bases (kb) on chromosome 2 and a deletion of about 150 kb on chromosome 3. The region of the deletion does not encode for any genes. However, the duplication includes a region with important developmental genes like *PAX3* and *EPHA4*, and thus the clone was excluded from further experiments. Interestingly, all WT clones except 18-3 showed duplications in the same region of chromosome 14, although generated from the same parental hiPSC line (passage ± 1) as the ko. Nevertheless, the clones were included as the olfactory receptor genes encoded in this genomic region have not been associated yet with development, DAns, or EN1. Further CNVs in clone 4-5 and 18-3 only affected a few (< 4) or no genes and were therefore also included. However, these clones must be used with caution and excluded if necessary. Clone 11-2 with a large duplication on chromosome 20 that encompassed more than 25 genes, including genes involved in apoptosis (*BCL2L1*) and the respiratory chain (*COX4I2*), was directly excluded from downstream experiments. This particular duplication has already been characterized as it was observed recurrently in hiPSCs. It results in a reduced level of apoptosis due to enhanced *BCL2L1* expression. As EN1 is a survival factor and is associated with mitochondrial dysfunction, the exclusion from further experiments is justifiable (Nguyen et al., 2014). In total, 3 *EN1* ko hiPSC lines as well as 5 WT hiPSC lines passed quality control and were used for further analysis (Table 2). Although subclones might not account for the same amount of variability as clones, cultivation of hiPSC subclones often results in mutations that can account for up to 10 % of the somatic mutations in hiPSCs. This suggests that there is an intrinsic variability not only in the selected clones but also in their subclones (D'Antonio et al., 2018).

As En1 is instrumental for the development and maintenance of DAns in mouse models, the hiPSCs were differentiated into neuronal cultures containing TH+ neurons to explore the impact of EN1 on DAn development in a human model. Neuronal cultures containing TH+ neurons

Table 2
Summary quality control. The generated hiPSC clones were subjected to quality control to ensure genomic integrity and pluripotency. The colony morphology, the expression of pluripotency markers (immunostaining), the differentiation into the three germ layers (immunostaining), and the karyotype (SNP microarray) were analyzed.

Subclone	Pluripotency markers			Tri-lineage differentiation						Karyotype
	SOX2	OCT4	NANOG	PAX6	NES	FOXA2	SOX17	TBXT	NCAM1	
5-6	✓	✓	✓	✓	✓	✓	✓	✓	✓	Normal
5-12	✓	✓	✓	✓	✓	✓	✓	✓	✓	Normal
25-19	✓	✓	✓	✓	✓	✓	✓	✓	✓	Normal
4-3	✓	✓	✓	✓	✓	✓	✓	✓	✓	196kb dup. Chr3
4-4	✓	✓	✓	✓	✓	✓	✓	✓	✓	196kb dup. Chr3
4-5	✓	✓	✓	✓	✓	✓	✓	✓	✓	171kb dup Chr3; 210kb del Chr1
15-1	✓	✓	✓	✓	✓	✓	✓	✓	✓	196kb dub Chr14
18-3	✓	✓	✓	✓	✓	✓	✓	✓	✓	368kb dub Chr7; 617kb dub Chr14

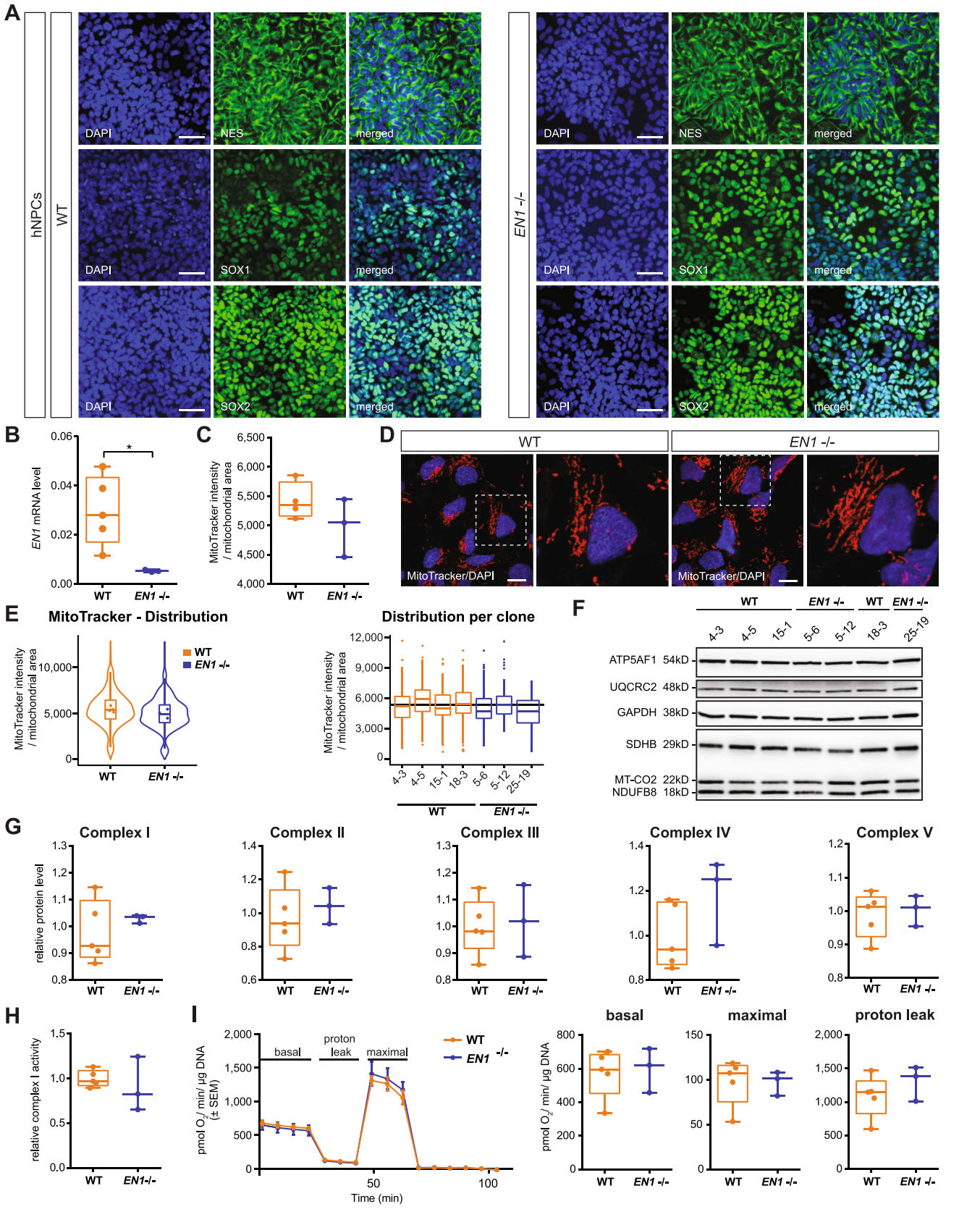

(caption on next page)

Fig. 3. *EN1* knock-out did not interfere with mitochondrial function in hNPCs.
(A) Immunofluorescence staining of hNPCs for the respective markers SOX1, SOX2, and NES are shown exemplarily for the WT clone 4-5, and the *EN1* ko clone 5-12. Scale bars: 50 μm.
(B) RT-qPCR analysis of *EN1* mRNA expression in hNPCs. mRNA levels were normalized to *ACTB*.
(C) MitoTracker staining to analyze mitochondrial functionality in hNPCs. The cytosolic fluorescence intensity was quantified.
(D) Staining is shown exemplarily for the WT clone 4-5, and the *EN1* ko clone 5-12. Scale bar: 10 μm.
(E) (left) Violin plots show the distribution of MitoTracker intensity per genotype (n = 100 cells/ clone). Dots indicate the mean values of individual clones. (right) Boxplots show the distribution for each clone individually.
(F) The abundance of mitochondrial complexes I - V was quantified by Western blot with antibodies against the labile subunits NDUFB8 (complex I), SDHB (complex II), UQCRC2 (Complex III), MT-CO2 (Complex IV), and ATP5F1A (Complex V). Expression levels were normalized to GAPDH. Western blots are exemplary shown for one replicate.
(G) Quantifications of protein levels of mitochondrial subunits are shown for hNPCs. Values were normalized to the average protein level of WT clones.
(H) Quantification of relative complex I activity. Complex I activity was normalized to the average activity of WT clones.
(I) Mitochondrial stress test performed in hNPCs using a Seahorse XFe96 Extracellular Flux Analyzer. An overview of the measurement (left) and detailed analyses of basal respiration, maximal respiration, and the proton leak is shown.
Experiments were performed in triplicates (n = 4-5 WTs and 3 *EN1* ko clones). Data are depicted as mean ± standard error of the mean (SEM) or box plots ranging from the 25th to 75th percentiles, showing the median. Whiskers extend from the min to max value or to the most extreme data point which is no more than 1.5 times the interquartile range (for E). Each dot represents one clone. p-values were determined by student's t-test (B), (C), (G), (H), (I), or a linear mixed effects model (E). $^{\#}p<0.1$; $^{*}p<0.05$; $^{**}p<0.01$; $^{***}p<0.001$.

were differentiated using a protocol adapted from (Reinhardt et al., 2013) for ventral CNS. In the first step, hiPSCs were differentiated into hNPCs. Finally, in a second step, hNPCs were further differentiated into neuronal cultures containing TH+ neurons.

hNPC identity was assessed by the expression of the markers SOX2, SOX1, PAX6, and NES (Fig. 3A). Developmentally, hNPCs can be staged before neural tube closure which correlates with E8.5 in mice. A developmental stage in which *En1* is already expressed. *EN1* expression was analyzed in hNPCs to validate the ko and the eligibility of hNPCs as a cellular model to investigate the molecular pathways associated with *EN1,* especially during the development of TH+ neurons. The *EN1* mRNA level was significantly reduced in *EN1* ko hNPCs compared to the WT control clones (Fig. 3B). Quantification at the protein level was not possible due to the lack of functional antibodies against EN1 for immunocytochemistry and WB. Interestingly, the expression of NPC markers was not affected, suggesting that EN1 is not required for the formation of hNPCs. Thus, hNPCs were used as a robust model to assess the molecular impact of EN1 on neuronal development.

2.2. The EN1 ko did not impact mitochondrial function in hNPCs

Injection of Engrailed in neurotoxic PD models demonstrated its neuroprotective effect, which is thought to be mediated amongst others by modulating mitochondrial function and stability (Alavian et al., 2014; Alvarez-Fischer et al., 2011). Therefore, mitochondrial integrity and cellular respiration were investigated to determine if the findings translated from mice into humans. At first, functional mitochondria were investigated using MitoTracker which accumulates specifically in mitochondria with an active membrane potential and thus an active and functional respiratory chain. In hNPCs, the *EN1* ko did not appear to affect overall mitochondrial functionality, as the average MitoTracker intensity per mitochondrial area was similar in WT and ko cells (Fig. 3C, D). Also, no clones or subpopulations were identified that exhibited different responses to the *EN1* ko (Fig. 3E). As subtle defects might have not been detected in the MitoTracker analysis, the integrity of the mitochondria with a focus on the respiratory chain was further investigated. The abundance of the respiratory chain complexes was analyzed by western blot for labile subunits of each complex (Fig. 3F, G). Although *EN1* has been described to regulate the expression of two complex I subunits, the relative protein level of complex I or any other respiratory chain complex was not altered in *EN1* ko hNPCs. Also, the activity of isolated complex I was similar in WT and *EN1* ko hNPCs (Fig. 3H). In line with this, the functionality of the respiratory chain determined by a mitochondrial stress test using the Seahorse XF system was not altered in *EN1* ko hNPCs (Fig. 3I).

In sum, this implies that the *EN1* ko did not alter complex I activity in human hNPCs nor the abundance of the respiratory complexes or cellular respiration per se.

2.3. Neurite arborization was altered during neuronal differentiation

In the next step, the hNPCs were further differentiated into neurons using a protocol generating also TH+ neurons. We did so to investigate the effect of the *EN1* ko on differentiation, maturation, and maintenance processes.

The efficiency of neuronal differentiation was estimated using immunostainings of the neuronal marker RBFOX3 (synonym: NeuN) and the single DAn marker TH. All except clone 15-1 were successfully differentiated into RBFOX3+ neurons and RBFOX3+/TH+ neurons (Fig. 4A). The differentiation efficiency into TH+ neurons was similar between *EN1* ko and WT cells (~8 %) as well as the percentage of RBFOX3+ neurons in the cultures (80 % - 90 %) (Fig. 4B). This might be due to a functional compensation by EN2, which is transcribed in *EN1* ko clones. This functional compensation of En2 has been investigated extensively in mice. In animal models, the phenotype of En1 mutants could be completely rescued by a knock-in of En2 into the En1 locus, which is normally expressed about 0.5 days later than En1 (Hanks et al., 1995; Simon et al., 2001). In contrast to the absence of a phenotype concerning DAn differentiation, the *EN1* ko resulted in the shortening of the average neurite length including the maximal neurite length with branches (**Fig. 4C**). Thus, this phenotype seems not to be compensated by En2.

2.4. The EN1 ko reduced mitochondrial function in neuronal cultures containing TH+ neurons

To further characterize the *EN1* ko phenotype on neuronal functionality, mitochondrial respiration was assessed. Contrary to the hNPCs, *EN1* ko neurons with ventral midbrain identity displayed reduced mitochondrial respiration already under homeostatic conditions (basal respiration), but also when forced to exhaust their full capacity (maximal respiration) (Fig. 4D). To determine alterations in the abundance of the respiratory chain complexes, western blots for labile subunits of each complex were performed. The abundance of complex III, and V was unchanged in *EN1* ko neuronal cultures, whereas the abundance of complex I, and IV was significantly reduced to about 60 % and levels of complex II tended to be reduced (Fig. 4E). The reduced abundance of complexes I and IV which are the main entry and exit points of the electron transport chain can explain the reduced mitochondrial respiration observed in Seahorse analysis. Deficits in complex I have been noticed predominantly in connection with *En1* ko mice, and impairments of complex IV regarding activity and abundance have also

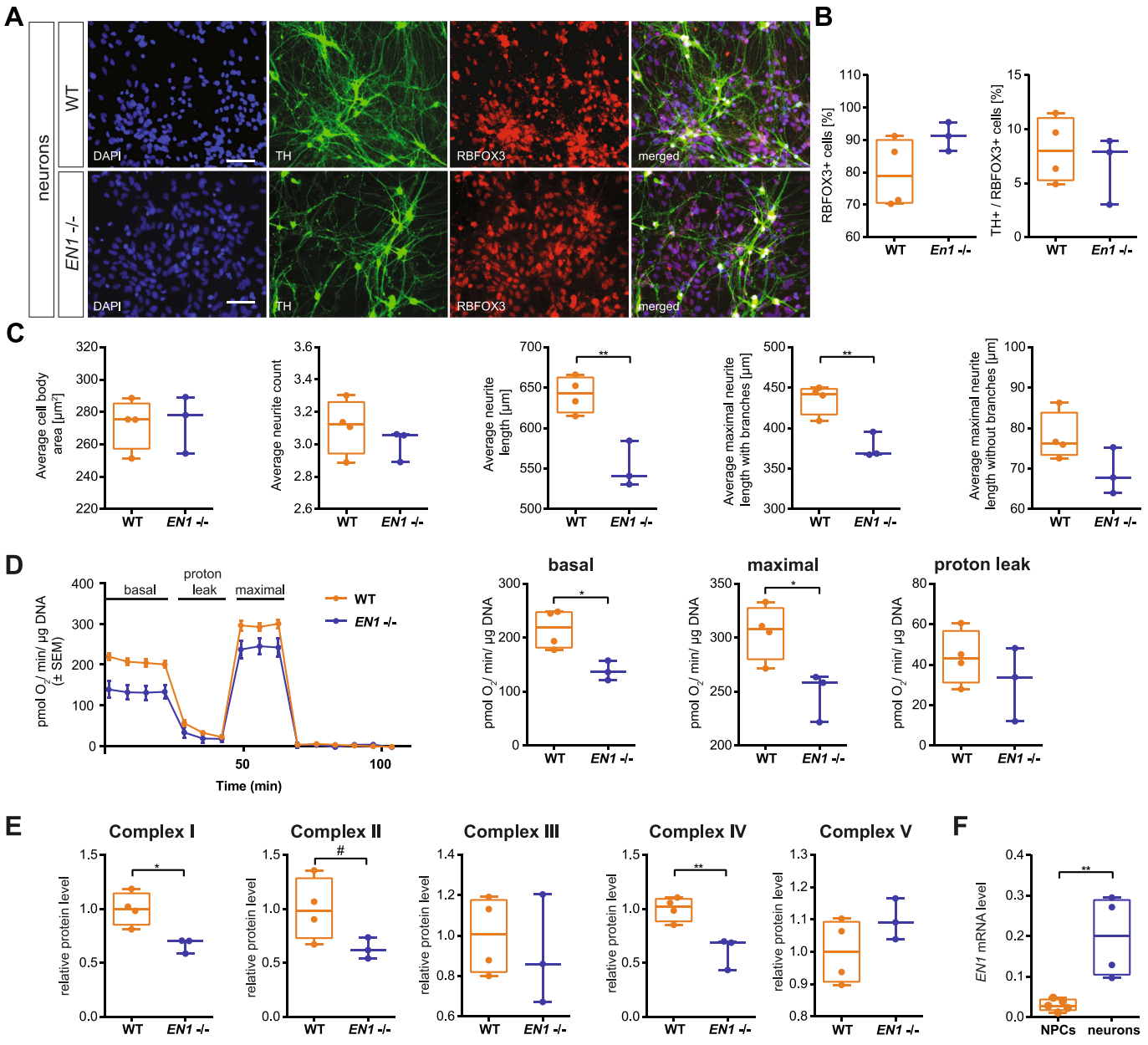

Fig. 4. *EN1* knock-out interferes with the arborization and mitochondrial function of neurons from cultures containing TH+ neurons.
(A) Immunofluorescence staining for neuronal marker RBFOX3 and the dopaminergic marker TH. Stainings are shown exemplarily for the WT clone 4-5, and the *EN1* ko clone 5-12. Scale bars: 50 µm.
(B) Quantification of RBFOX3 (synonym: NeuN) positive as well as TH / RBFOX3 double-positive cells in neuronal populations.
(C) Characterization of neurite morphologies of TH+ neurons. Boxplots show the average size of TH-positive cell bodies, the number of neurites emerging from these cell bodies, their average length, as well as their maximal length with and without branches.
(D) Mitochondrial stress test performed in neuronal cultures containing TH+ neurons using a Seahorse XFe96 Extracellular Flux Analyzer. (left) An overview of the measurement and (right) detailed analyses of basal respiration, maximal respiration, and proton leak are shown, respectively.
(E) Analysis of complex I-V abundance by western blot in neuronal cultures containing TH+ neurons using antibodies against NDUFB8 (complex I), SDHB (complex II), UQCRC2 (Complex III), MT-CO2 (complex IV) and ATP5A (complex V). Protein levels were normalized to ACTB or GAPDH and the average protein levels of WT clones.
(F) RT-qPCR analysis of *EN1* mRNA expression in WT hNPCs and in neuronal cultures containing TH+ neurons. mRNA levels were normalized to *ACTB*.
Experiments were performed in triplicates, using three independent differentiations (n = 4 WTs and 3 *EN1* ko clones). Data are depicted as mean ± standard error of the mean (SEM) or box plots ranging from the 25th to 75th percentiles, showing the median. Whiskers extend from min to max value and each dot represents one clone. p-values were determined by student's t-test. $^{\#}p<0.1$; $^{*}p<0.05$; $^{**}p<0.01$; $^{***}p<0.001$.

been observed in PD models (Martin et al., 2006; Palacino et al., 2004; Subramaniam and Chesselet, 2013). That mitochondrial alterations were detectable in neurons but not hNPCs might be due to the strong upregulation of *EN1* expression during the differentiation process and/or the different cell types (Fig. 4F).

In sum, the effect of the *EN1* ko was prominent in neurons which exhibited an increased *EN1* expression in WT neurons if compared to WT hNPCs. The *EN1* ko resulted in reduced mitochondrial respiration, reduced levels of subunits of the electron transport chain, as well as alterations in neurite arborization.

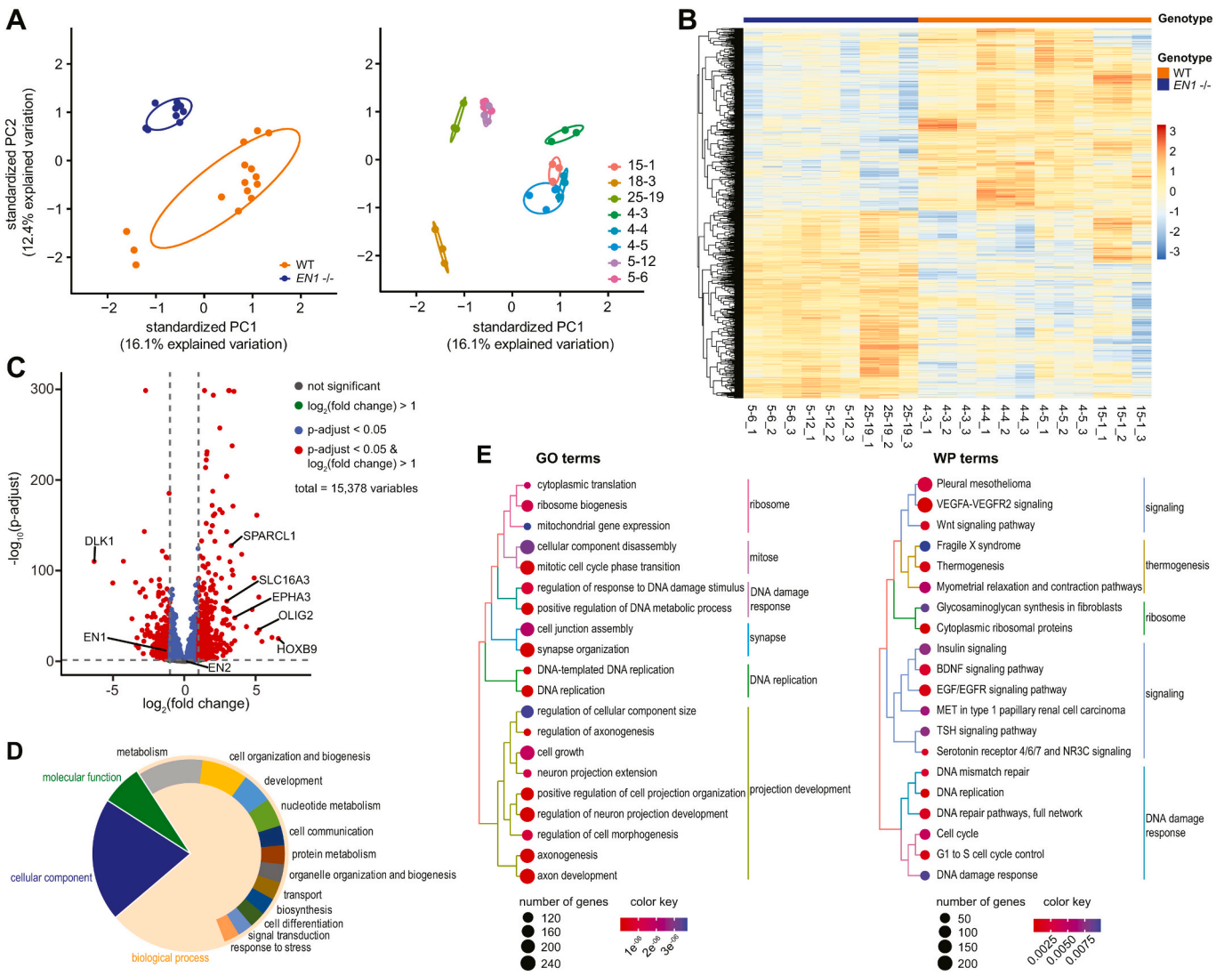

Fig. 5. Transcriptome analysis highlights the relevance of EN1 for neuronal outgrowth and cellular signaling.
(A) Transcriptome analysis of hNPCs. Principal component analysis visualizes the variability within (right) technical replicates and (left) genotype conditions and of individual samples. Probability ellipses depict 0.68 of normal probability.
(B) Heatmap summarizing log2 transformed fold changes with rows scaled by z-score for differentially expressed genes (DEGs).
(C) Volcano plot shows DEGs according to their fold change and significance. Every detected gene is represented by a dot. Lines visualize fold change ($\log_2(0.5)$) and significance ($-\log_2(0.05)$) cut-offs. Selected genes are highlighted.
(D) Classification of significantly enriched GO terms. GO annotations were further analyzed for gene function groups within the main category 'biological process'.
(E) Tree plots of the pathway enrichment analysis show significantly enriched (left) GO and (right) WikiPathway terms. p-values were determined by one-sided hypergeometric tests. FDR-corrected p-values are represented by q-values.

2.5. Transcriptome analysis links EN1 to neurite arborization and cellular signaling

hNPCs "primed" (see Material and Methods) to differentiate into DAns represent a robust model to screen for the *EN1* ko-induced molecular alterations during the development of DAns. This is of great importance for the developmental function of EN1. During the early phase of expression, Engrailed is crucial for the correct mid-/hindbrain patterning (Liu and Joyner, 2001), axon guidance (Fuchs et al., 2012), and later on for the maintenance of DAns (Albéri et al., 2004; Simon et al., 2001). To explore the molecular consequences of the *EN1* ko explicitly during DAn differentiation in an unbiased way, transcriptome analysis of *EN1* ko and WT hNPCs was performed. mRNA was collected from all *EN1* ko and WT clones in triplicates.

Dimensionality reduction of the transcriptome data was performed using principal component analysis (PCA). PCA enables the visualization of variations and similarities between samples and replicates to identify possible outliers. The observed variation between technical replicates is lower than the variation between different clones. Furthermore, the highest variance (PC1) could be attributed to the genotype (Fig. 5A). However, one WT clone (18-3) clustered separately and was thus removed as an outlier for downstream analysis (Fig. 5A and Fig. S1A).

A total of 15,378 features were identified of which 7,702 were significantly dysregulated (p-adjust < 0.05) (Table S2). A heatmap summarizing the differentially expressed genes (DEGs) is shown in Fig. 5B. However, the majority of DEGs were slightly dysregulated with only 801 DEGs having an absolute log2 fold change larger than 1, including *EN1* (log2 fold change = -1.29; p-adjust = $3.5*10^{-12}$). This is in line with the RT-qPCR results reported above (Fig. 3B) and further validates the knock-out. Furthermore, the number of DEGs that were upregulated (3,910 – 50.8 %) or downregulated (3,792 – 49.2 %) due to the *EN1* ko was more or less balanced (Fig. 5C).

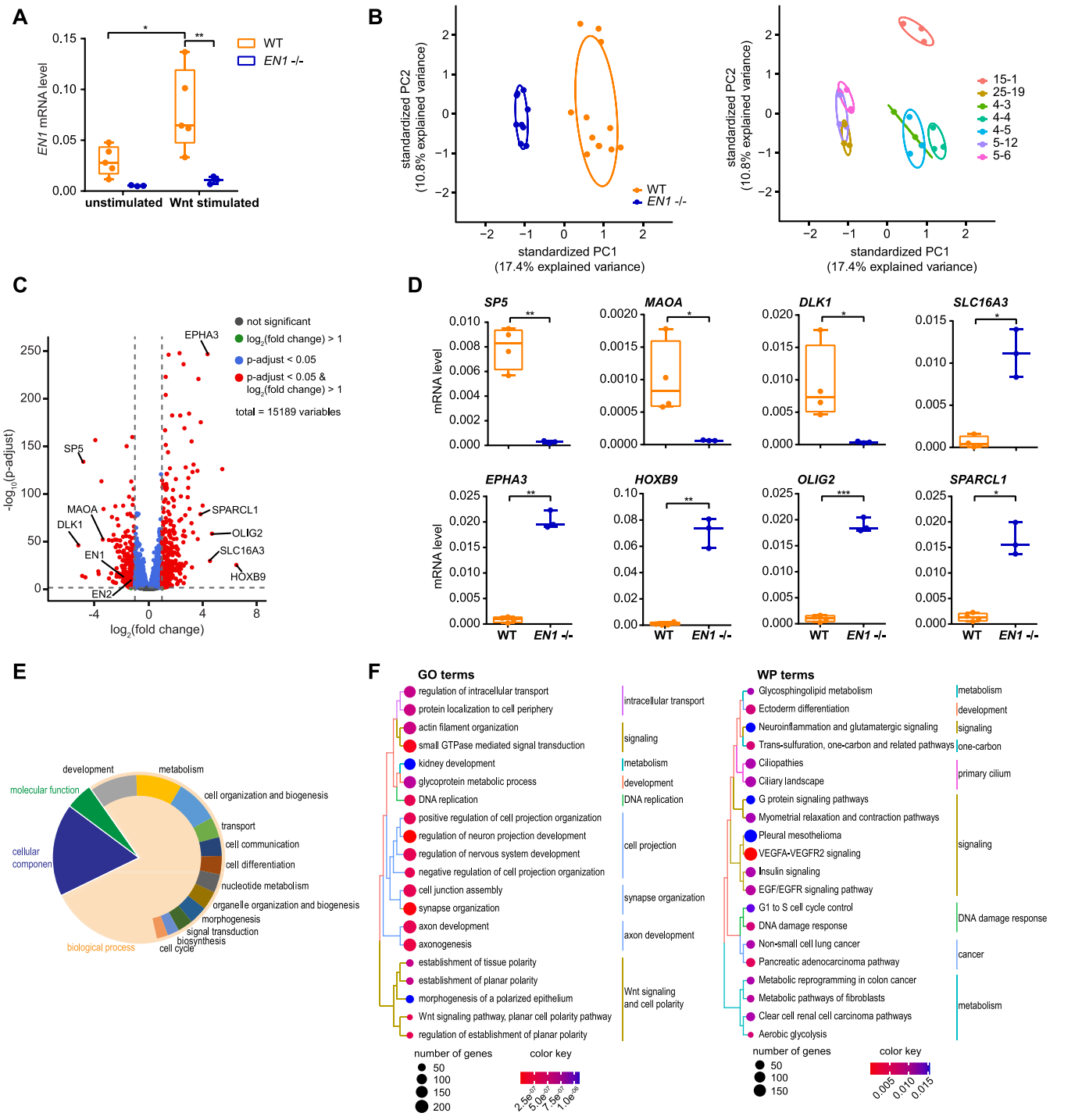

Fig. 6. Wnt stimulation increased *EN1* expression and enhanced the misregulation of primary cilia related pathways.
(A) RT-qPCR analysis of *EN1* mRNA expression in unstimulated and Wnt stimulated (3 μM CHIR99021 for 48h) hNPCs. mRNA levels were normalized to *ACTB*.
(B) Transcriptome analysis of Wnt stimulated hNPCs (3 μM CHIR99021 for 48h). Principal component analysis visualizes the variability within (right) technical replicates and (left) genotype conditions and of individual samples. Probability ellipses depict 0.68 of normal probability.
(C) Volcano plot shows DEGs according to their fold change and significance. Every detected gene is represented by a dot. Lines visualize fold change ($\log_2(0.5)$) and significance ($-\log_2(0.05)$) cut-offs. Selected genes are highlighted.
(D) Misexpression of the top DEGs *SP5, MAOA, DLK1, SLC16A3, EPHA3, HOXB9, OLIG2, SPARCL1* was validated using RT-qPCR analysis. mRNA levels were normalized to *ACTB*.
(E) Classification of significantly enriched GO terms. GO annotations were further analyzed for gene function groups within the main category 'biological process'.
(F) Tree plots of the pathway enrichment analysis show significantly enriched (left) GO and (right) WikiPathway terms. p-values were determined by one-sided hypergeometric tests. FDR-corrected p-values are represented by q-values.
Experiments were performed in triplicates, using three independent differentiations (n = 4 WTs and 3 EN1 ko clones). Data are depicted as box plots ranging from the 25th to 75th percentiles, showing the median. Whiskers extend from min to max value and each dot represents one clone. p-values were determined by student's t-test (A), (D). $^{\#}p<0.1$; $^{*}p<0.05$; $^{**}p<0.01$; $^{***}p<0.001$.

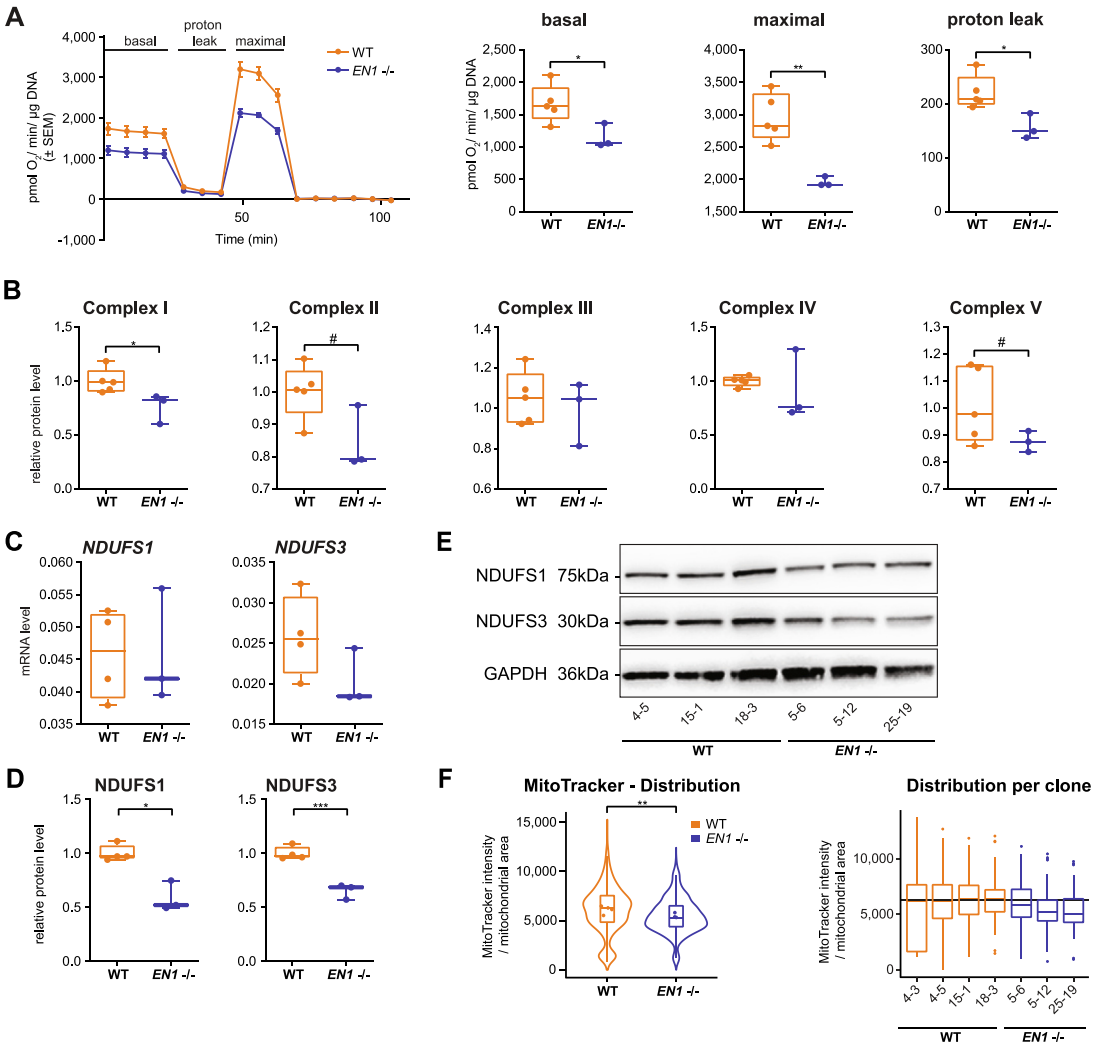

Fig. 7. Wnt stimulation interfered with mitochondrial function in *EN1* knock-out hNPCs.
(A) Mitochondrial stress test performed in Wnt stimulated hNPCs (3 µM CHIR99021 for 48h) using a Seahorse XFe96 Extracellular Flux Analyzer. An overview of the measurement (left) and detailed analyses of basal respiration, maximal respiration, and the proton leak is shown, respectively.
(B) The abundance of mitochondrial complexes I - V was quantified by Western blot with antibodies against the labile subunits NDUFB8 (complex I), SDHB (complex II), UQCRC2 (Complex III), MT-CO2 (Complex IV), and ATP5F1A (Complex V). Quantifications of protein levels are shown for Wnt-stimulated hNPCs. Expression values were normalized to GAPDH and to the average protein level of WT clones.
(C) Normalized gene expression levels of the mitochondrial complex I subunits *NDUFS1* and *NDUFS3* analyzed on mRNA level by RT-qPCR and
(D) on protein level by Western blot in Wnt stimulated hNPCs (3 µM CHIR99021 for 48h). Values were normalized to the average protein level of WT clones.
(E) The abundance of the mitochondrial complex I subunits NDUFS1 and NDUFS3 was quantified using Western blot. Expression levels were normalized to GAPDH. Western blots are exemplary shown for one replicate.
(F) MitoTracker staining was used to quantify functional mitochondria in Wnt-stimulated hNPCs (3 µM CHIR99021 for 48h). The cytosolic fluorescence intensity was quantified. (left) Violin plots show the distribution of MitoTracker intensity per genotype (n = 100 cells/ clone). Dots indicate the mean values of individual clones. (right) Boxplots show the distribution for each clone individually.
Experiments were performed in triplicates (n = 4-5 WTs and 3 *EN1* ko clones). Data are depicted as mean ± standard error of the mean (SEM) or box plots ranging from the 25th to 75th percentiles, showing the median. Whiskers extend from the min to max value or to the most extreme data point which is no more than 1.5 times the interquartile range (for F). p-values were determined by student's t-test (A), (B), (C), (D), or a linear mixed effects model (F). $^{\#}p<0.1$; $^{*}p<0.05$; $^{**}p<0.01$; $^{***}p<0.001$.

To analyze the molecular changes introduced by the *EN1* ko, pathway enrichment analysis was performed using multiple databases (**Fig. 5D, E**; Fig. S1B; Table S3). The vast majority (73.0 %) of significantly enriched GO Terms were associated with the category 'biological process' including many 'metabolism'/'nucleotide metabolism', 'cell organization and biogenesis', as well as 'development' associated terms (Fig. 5D). The top 20 enriched terms were mainly associated with 'projection development', next to 'ribosome' functionality, 'DNA replication', and the 'DNA damage response' (Fig. 5E). Contrary, the top WikiPathways terms were mainly associated with cellular 'signaling', including the 'Wnt signaling pathway' (Fig. 5E), but also included many terms associated with the 'DNA damage response'.

These pathways match with known functions of *EN1*, for example in synapse physiology (Di Nardo et al., 2007; Marie et al., 2000; Pézier et al., 2014), axon guidance during development (Nédélec et al., 2004; Saueressig et al., 1999), and axon maintenance (Nordströma et al., 2015). Furthermore, EN1 has also been association with the Wnt pathway before (Danielian and McMahon, 1996). The fact that most pathways could be related to established functions of En1 across different organisms suggests a conserved role of EN1 also in humans. Interestingly, the association of En1 with mitochondria and complex I which is thought to partially mediate its neuroprotective function was

also not reflected in the transcriptome data. This is in line with the respiratory characterization of the *EN1* ko hNPCs (Fig. 3).

2.6. Wnt stimulation unmasked EN1 ko-induced alterations in cellular transport and signaling

As a deficit in mitochondrial respiration could be identified in *EN1* knock-out neuronal cultures containing TH+ neurons but not in *EN1* knock-out hNPCs might indicate that the level of EN1 was not high enough in hNPCs to trigger a detectable effect on mitochondrial function yet. As described before, *EN1* expression can also be induced by Wnt1 signaling, which has been described in different species (Danielian and McMahon, 1996; Kim et al., 2018; McGrew et al., 1999). The regulation is direct via the Tcf/Lef components of the Wnt pathway (Kim et al., 2018). In addition, the transcriptome data identified DEGs in the Wnt signaling pathway which further implied a connection between EN1 and Wnt signaling (Fig. 5E). Therefore, to increase the *EN1* expression in hNPCs and enhance the effect of the knock-out, hNPCs were stimulated for 48h with 3 μM CHIR99021. CHIR99021 is a GSK-3β inhibitor that inhibits the phosphorylation and degradation of β-catenin and thus induces the expression of Wnt target genes. As expected, the *EN1* mRNA level was significantly increased upon Wnt stimulation in WT hNPCs, whereas the stimulation did not affect *EN1* expression in *EN1* ko hNPCs (Fig. 6A).

To assess the consequences of the *EN1* knock-out in the enhanced model in an unbiased way, transcriptome analysis was performed using Wnt-stimulated hNPCs. PCA showed again that the variation between replicates was low and the highest variability (17.4 %) within the transcriptome dataset could be attributed to the genotype (Fig. 6B). Based on the PCA and the correlations between clones (Fig. S2A), no outliers were removed for downstream analysis.

A total of 15,189 features were identified of which 6,581 were significantly dysregulated (p-adjust < 0.05) between Wnt stimulated WT and *EN1* ko hNPCs (Table S4). A heatmap summarizing the DEGs is shown in Fig. S2B. Again, the majority of differentially expressed genes (DEGs) were slightly dysregulated with only 699 DEGs having an absolute log2 fold change larger than 1, including *EN1* (log2 fold change = -1.84; p-adjust = $4.3*10^{-13}$). Furthermore, the number of DEGs that were upregulated (3,259 – 49.5 %) or downregulated (3,322 – 50.5 %) due to the *EN1* ko was more or less balanced as also indicated by the volcano plot (Fig. 6C). To validate the outcome of the transcriptome analysis, the mRNA levels of top up- and downregulated DEGs were verified by RT-qPCR (Fig. 6D).

Subsequently, a pathway enrichment analysis was performed to investigate the molecular alterations in Wnt-stimulated *EN1* ko cells in comparison to the WT cells using multiple databases (Fig. 6E, F; Fig. S2C; Table S5). As for the unstimulated dataset, the vast majority (77.5 %) of significantly enriched GO terms were associated with the category 'biological process', including many 'development', 'metabolism', 'cell organization and biogenesis', and now also 'transport' associated terms (Fig. 6E). Due to the Wnt stimulation, the proportion of 'development' terms increased by 73.8 %, of 'transport' terms by 29.6 %, and of 'cell differentiation' terms by 28.5 %. Contrary, the proportion of 'metabolism' and 'biosynthesis' associated terms was dramatically reduced. Accordingly, the top 20 enriched terms now also included 'intracellular transport' and 'protein localization' terms next to the 'neurite projection' related terms (Fig. 6F). Again, the top WikiPathways terms were mainly associated with cellular 'signaling', but now also included terms related to 'primary cilia' or 'ciliopathies' (Fig. 6F). Unexpectedly, again no OXPHOS or mitochondria-associated pathways were enriched in Wnt stimulated *EN1* ko hNPCs. Thus, even with an increased *EN1* expression, transcriptome analysis did not suggest defects in the respiratory chain or mitochondrial function per se.

In sum, the *EN1* expression could be increased in hNPCs using Wnt stimulation. These additional transcriptome data strengthen the link between EN1 and neurite arborization, as well as cellular signaling. However, also under this condition, the *EN1* ko did not affect OXPHOS or mitochondria-related pathways on the transcriptome level.

2.7. Metabolic deficits develop in Wnt stimulated EN1 ko hNPCs

Although mitochondrial pathways were not affected on the transcriptome level, these findings do not necessarily exclude metabolic alterations. The connection between EN1 and PD, as well as the neuroprotective effect of EN1 is thought to be mainly mediated by adapting mRNA translation especially of mitochondrial complex I subunits such as Ndufs1 and Ndufs3 (Alvarez-Fischer et al., 2011). Thus, we investigated mitochondrial functionality also in Wnt-stimulated hNPCs that exhibited an increased *EN1* expression.

Contrary to the unstimulated cells, mitochondrial respiration was significantly reduced in Wnt-stimulated *EN1* ko hNPCs. These hNPCs exhibited a decreased mitochondrial respiration already under homeostatic conditions (basal respiration), which became more pronounced when forced to work with full capacity (maximal respiration) (Fig. 7A). The proton leak was also reduced in *EN1* ko hNPCs. Overall, Wnt stimulation seemed to affect more severely WT cells, whereas *EN1* ko cells only reacted slightly to adapt their mitochondrial respiration (Fig. S3A) upon stimulation. This is concordant with Wnt being upstream of EN1 and implies a genotype-related dysfunction.

To detect the molecular alterations underlying the mitochondrial deficiency in the *EN1* ko hNPC, the abundances of the respiratory chain complexes were analyzed by western blot, as EN1 is known to enhance the translation of the mitochondrial complex I subunits Ndufs1 and Ndufs3 (Alvarez-Fischer et al., 2011). Indeed, Wnt stimulation revealed a decreased abundance of complex I in *EN1* ko cells, while the abundances of the remaining respiratory chain complexes were mainly unchanged (Fig. 7B). Next to reduced levels of the labile subunit NDUFB8 (Fig. 7B), also protein levels of NDUFS1 and NDUFS3 were significantly reduced in *EN1* ko hNPCs following Wnt stimulation (Fig. 7D, E). However, as indicated by the transcriptome analysis and validated by RT-qPCR analysis (**Fig. 7C**), the expression of *NDUFS1* and *NDUFS3* was not affected on the transcriptome level.

Additionally, the functionality of mitochondria was assessed by MitoTracker staining. Mitochondria seemed to be less active in Wnt-stimulated *EN1* ko clones (Fig. 7F). Distribution analysis revealed that more Wnt-stimulated *EN1* ko cells displayed a significantly reduced fluorescence intensity per mitochondrial area then stimulated WT cells. As the total area of mitochondria (Fig. S3B) was unchanged between *EN1* ko and WT hNPCs after Wnt-stimulation, the reduced intensity can be attributed to a reduced membrane potential rather than decreased functional mitochondrial mass. Similar to the Seahorse analyses, the *EN1* ko lines again appeared to fail to adapt their metabolism in response to Wnt stimulation. The MitoTracker intensity was increased in WT hNPCs upon Wnt stimulation but remained at lower levels in *EN1* ko cells (Fig. S3C).

These changes in complex I abundance and the overall membrane potential can explain the reduced mitochondrial respiration observed in the mitochondrial stress test for Wnt-stimulated *EN1* ko hNPCs. Furthermore, the observed alterations on the proteome but not on the transcriptome level match the described EN1 function of being a post-transcriptional regulator (Alvarez-Fischer et al., 2011).

2.8. Impact of Wnt stimulation on the transcriptome of WT and EN1 ko hNPCs

To determine the effect of the Wnt signaling on the transcriptome of *EN1* ko or WT hNPCs, respectively, the transcriptome data of unstimulated versus Wnt-stimulated hNPCs were compared for both *EN1* ko and WT cells. As expected, when comparing the unstimulated with the Wnt stimulated dataset, the highest variation (PC1 – 17.8 % variation) was now attributed to the stimulation and not the different genotypes anymore, which, however, still accounted for 10.6 % (PC2) of the

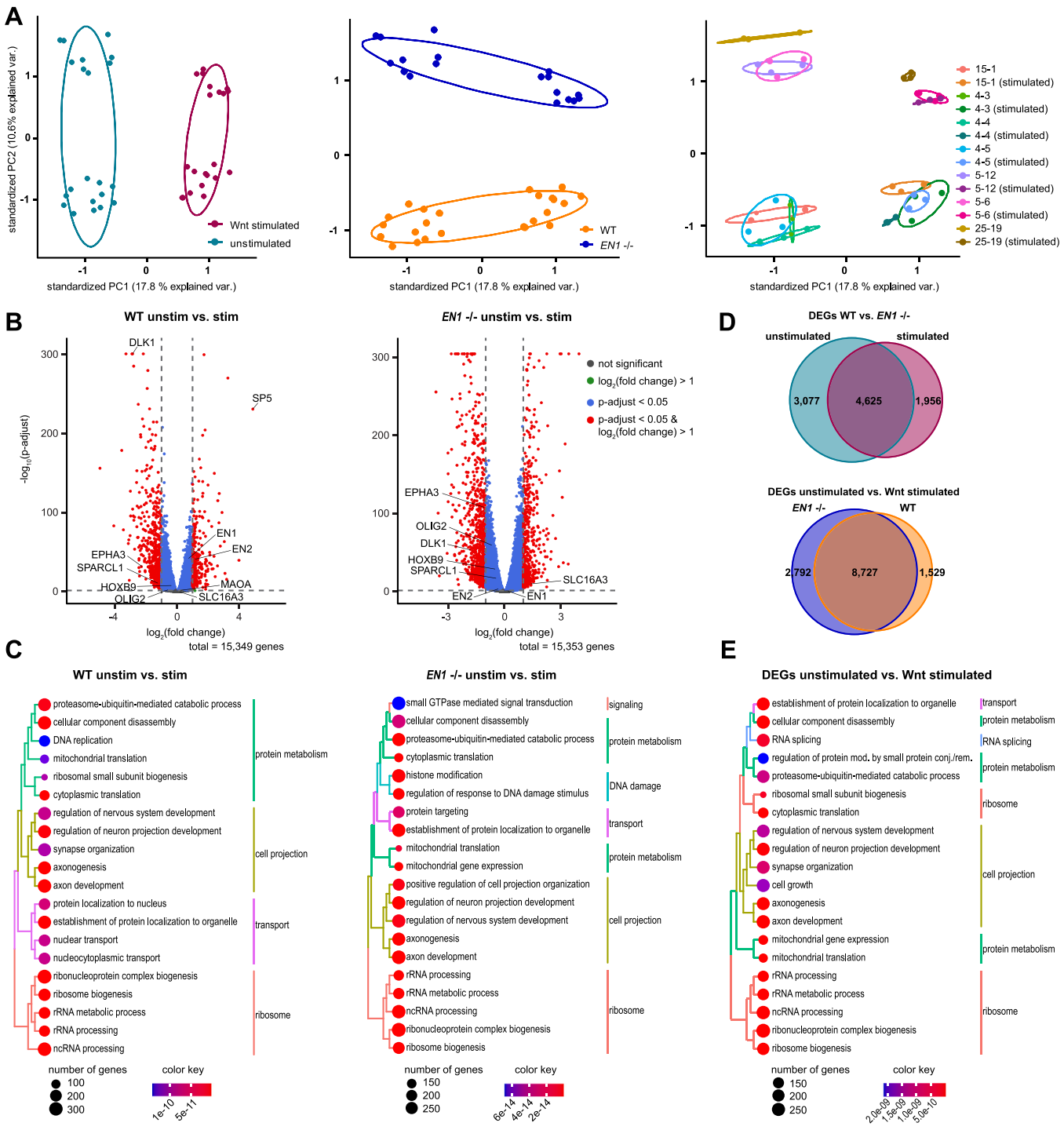

Fig. 8. Impact of Wnt stimulation on the transcriptome of WT and *EN1* ko hNPCs

(A) Principal component analysis visualizes the variability within (right) technical replicates, (middle) genotype conditions, (left) and stimulation conditions. Probability ellipses depict 0.68 of normal probability.

(B) Volcano plots show DEGs according to their fold change and significance. Every detected gene is represented by a dot. Lines visualize fold change ($\log_2(0.5)$) and significance ($-\log_2(0.05)$) cut-offs. Selected genes are highlighted.

(C) Tree plots of the pathway enrichment analysis show significantly enriched GO terms. p-values were determined by one-sided hypergeometric tests. FDR-corrected p-values are represented by q-values.

(D) (top) Overlap of DEGs (WT vs. *EN1* ko) in the unstimulated and stimulated dataset, (bottom) as well as of the DEGs (unstimulated vs. stimulated) for the WT and the *EN1* ko samples.

(E) Tree plot of the pathway enrichment analysis show significantly enriched GO terms. p-values were determined by one-sided hypergeometric tests. FDR-corrected p-values are represented by q-values.

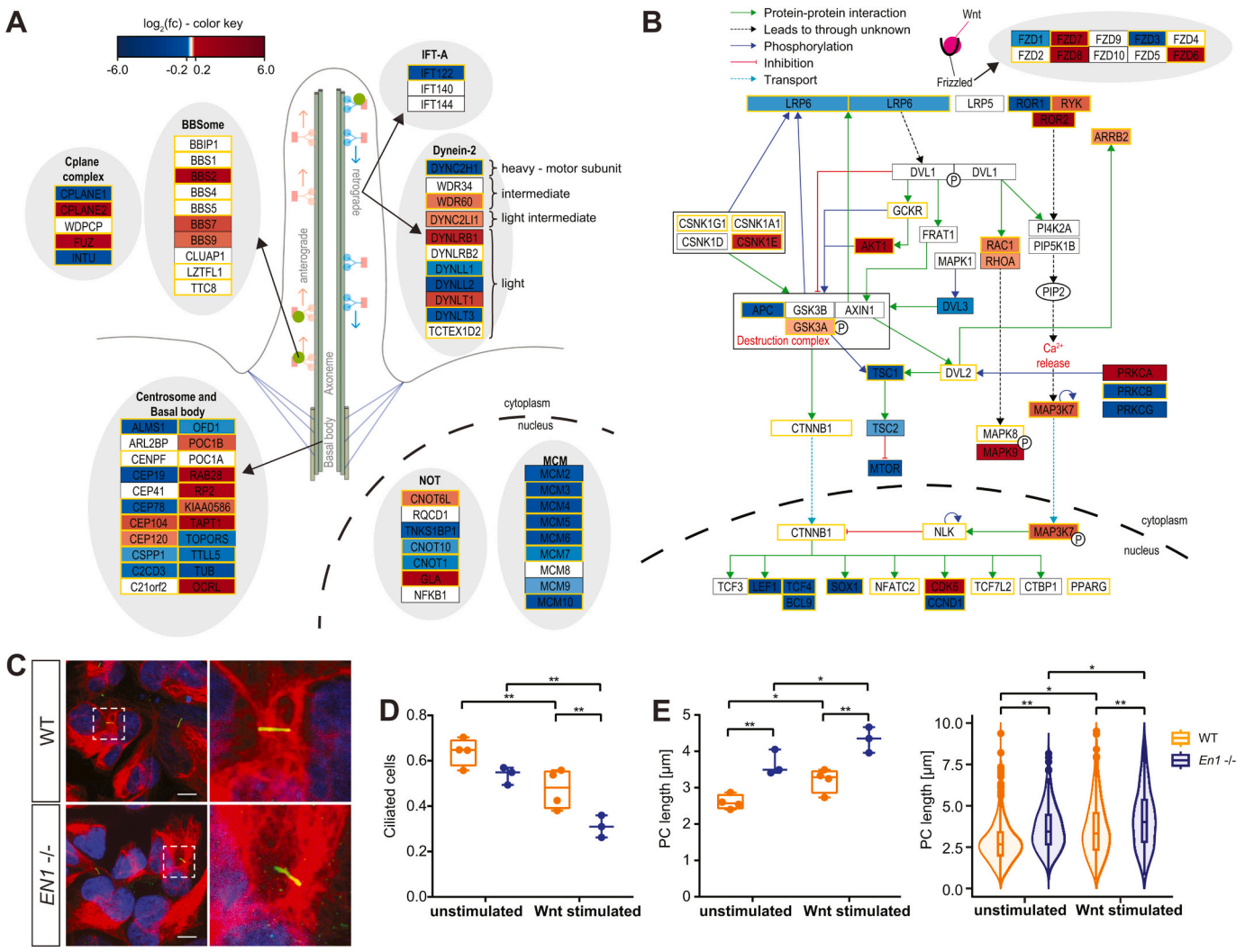

Fig. 9. *EN1* knock-out impairs ciliogenesis and primary cilia morphology.
(A) Visualization of the WikiPathways terms 'Ciliary landscape' and **(B)** 'Wnt signaling pathway'. For (A) and (B), visualizations are based on the transcriptome data from Wnt stimulated hNPCs (3 µM CHIR99021 for 48h) with manual annotations. Up- (red) and downregulated (blue) DEGs are sorted into functional categories. Color intensity is proportional to the fold change. Genes that were significantly dysregulated (same direction) in both the unstimulated and the Wnt-stimulated data sets were highlighted in yellow.
(C) Immunofluorescence staining for the NPC marker NES (red) together with the PC marker ARL13B (green). Nuclei were stained using DAPI (blue). Staining is exemplarily shown for the WT clone 4-5, and the *EN1* ko clone 5-12. Scale bars: 10 µm.
(D) Fraction of ciliated hNPCs in unstimulated and Wnt stimulated (3 µM CHIR99021 for 48h) populations.
(E) PC length was measured in immunostainings of hNPCs positive for NES and ARL13B. (left) Average PC length per clone. (right) Violin plots illustrate the distribution of PC length per condition. n=50-80 cilia per clone.
Experiments were performed in triplicates (n = 4-5 WTs and 3 *EN1* ko clones). Boxplots display the median and range from the 25th to 75th percentile. Whiskers extend from the min to max value or to the most extreme data point which is no more than 1.5 times the interquartile range (for E (right)). Each dot represents one clone. p-values were determined by one-way ANOVA with Sidak's post hoc test (D), (E left) or a linear mixed effects model (E right). $^{\#}p<0.1$; $^{*}p<0.05$; $^{**}p<0.01$; $^{***}p<0.001$.

variation (Fig. 8A). Consequently, high numbers of DEGs could be identified for the comparison of unstimulated with Wnt stimulated hNPCs with 10,256 (out of 15,349 total features) for the WT hNPCs or 11,519 (out of 15,353 total features) for the *EN1* ko, which is roughly 2/3 of the whole transcriptome (Fig. 8B; Table S6). Still, the majority of DEGs were only weakly dysregulated due to the Wnt stimulation with an absolute log2 fold change of less than 1, and only 851 DEGs in WT or 1,393 in *EN1* ko hNPCs exhibited a larger absolute log2 fold change (Table S6). Thus, *EN1* ko hNPCs seemed to be more responsive to Wnt stimulation, at least in terms of transcriptional changes, with 1.64 times more genes being strongly dysregulated.

Comparing the gene expression data of unstimulated WT hNPCs with Wnt-stimulated WT hNPCs allowed the identification of DEGs that were mainly enriched in GO terms associated with 'ribosome biogenesis', especially 'rRNA processing', with 'protein metabolism', 'nuclear transport', and 'cell projections' (Fig. 8C; Table S7). Similar processes seemed to be affected in *EN1* ko hNPCs upon Wnt stimulation. Additionally, pathways associated with 'DNA damage' and 'signal transduction' were affected (Fig. 8C; Table S8). Interestingly, the top KEGG terms for the *EN1* ko DEGs were also associated with 'Parkinson's disease' and neurodegenerative diseases. Also for WT hNPCs, KEGG terms associated with 'Parkinson's disease' and neurodegenerative diseases were significantly affected, however, not to a similar extent as for the *EN1* ko hNPCs with roughly 25 % fewer associated DEGs. Thus, Wnt stimulation seemed to result in a general interference with the expression of Parkinson's Disease associated genes, which was more

pronounced on an *EN1* ko genetic background.

Besides that, the DEGs for the comparison of the unstimulated to the Wnt stimulated sets were quite similar for WT and *EN1* ko hNPCs with 8,727 DEGs being dysregulated in both genotypes (Fig. 8D; Table S6), and 7,804 DEGs (89 % of the overlap) were dysregulated in the same direction. Consequently, these DEGs were associated with similar GO terms related to 'ribosome biogenesis', 'protein metabolism', 'cell projection', 'RNA splicing', and 'transport' (Fig. 8E; Table S9).

Based on the transcriptome analysis, Wnt stimulation did not seem to affect hNPC differentiation processes differently in WT and *EN1* ko hNPCs in our cultures, if they were altered at all under these conditions.

2.9. Primary cilia are impaired in EN1 ko hNPCs

Especially interesting was also the finding of enriched terms associated with primary cilia in the transcriptome analysis. Primary cilia are microscopic, hair-like cellular organelles that extend from the cell surface. They are thought to function as 'signaling antennae' that receive and process signals from the extracellular environment, and by transmitting these signals to the cytoplasm and nucleus, they control gene expression and cellular pathways. Primary cilia contain 9 pairs of microtubules, the axoneme, which are connected to the mother centriole also referred to as the basal body. The axoneme is surrounded by the cell membrane on the remaining sides. Based on the transcriptome analysis, various ciliary processes summarized in the WikiPathways term 'ciliary landscape' were affected in *EN1* ko hNPCS, especially following Wnt stimulation. Selected processes are visualized in Fig. 9A together with their associated DEGs. Interestingly, mainly two ciliary processes were thereby severely affected and also similarly dysregulated in both the unstimulated and the Wnt stimulated dataset namely the CPLANE complex, and the minichromosome maintenance protein complex (MCM). The CPLANE complex is linked to intraflagellar transport processes, planar cell polarity as well as SHH signal transduction. Deficiency of the CPLANE complex thereby leads to defective ciliogenesis and thus ciliopathies (Martín-Salazar and Valverde, 2022). The MCM has been suggested to interact with the centrioles to promote ciliogenesis (Casar Tena et al., 2019; Ferguson et al., 2010; Stuermer et al., 2007; Tingler et al., 2022).

Based on these observations, an impairment of ciliogenesis due to the *EN1* ko can be assumed, especially in hNPCs following Wnt stimulation. Indeed, upon Wnt stimulation, the fraction of ciliated cells was significantly reduced in *EN1* ko hNPCs to 31 % compared to WT hNPCs with a fraction of 48 % (Fig. 9C, D). With a reduced ciliogenesis, however, average cilia length was increased in *EN1* ko hNPCs by 35 % to 4.3µm on average (Fig. 9E).

In order to fulfill their function as cellular 'signaling antenna', membrane-bound receptors as well as proteins involved in signal transduction are enriched in the ciliary membrane or lumen. During the signal transduction events, primary cilia are mainly involved in the post-translational processing of the respective downstream mediators, also in the case of SHH and Wnt signaling. The other way around, it has also been shown that canonical Wnt signaling mediated by Wnt3a can promote ciliogenesis in MCF-7/ADR cells (Kyun et al., 2020). Conversely, however, ciliogenesis was reduced, but cilia length was increased in both WT and *EN1* ko hNPCs following Wnt stimulation (Fig. 9D, E). As many genes involved in the transduction of Wnt signaling were already dysregulated in unstimulated *EN1* ko hNPCs (Fig. 9B), it is reasonable to assume that EN1 is also necessary for the fine-tuning of Wnt signaling. In line with this, *EN1* ko hNPCs responded more severely than WT cells to Wnt stimulation (Fig. 9D, E). Nevertheless, already in unstimulated *EN1* ko hNPCs cilia length was significantly increased, whereas ciliogenesis was not affected (Fig. 9D, E). This indicates an involvement of *EN1* in ciliary processes determining cilia length, such as protein sorting or intraflagellar transport.

In sum, Wnt stimulation resulted in a slightly reduced ciliogenesis in WT hNPCs and a significant elongation of primary cilia. This phenotype was even enhanced in *EN1* ko hNPCs, indicating an involvement of EN1 in primary cilia function due to Wnt signaling.

3. Discussion

The etiology of PD remains – despite PD being known for such a long time – still highly elusive. In the last two decades, however, animal models carrying mutations in PD-associated genes (e.g. *Pink1*, *Lrrk2*, *DJ-1*) have been established (Giesert et al., 2017; Glasl et al., 2012; Goldberg et al., 2005; Seegobin et al., 2020; Wang et al., 2008). Even though none of these model precisely recapitulated PD pathology, they still provided valuable information that contributed to our understanding of the disease pathology, which by now is known to include dysfunctional protein aggregation, mitochondria, and autophagy (Giguère et al., 2018; Poewe et al., 2017; Schmidt et al., 2022b; Surmeier et al., 2017). The recapitulation of the progressive loss of DAns is, however, only reproducible in mouse models exhibiting heterozygosity for En1 (Nordströma et al., 2015; Sonnier et al., 2007). En1 contributes to the signaling and transcriptional pathways required for the proper embryonic development of DAns but is still active in the adult mammalian midbrain and its adult activity seems to have neuroprotective functions. This is also supported by the discovery of single nucleotide polymorphisms in *EN1* which increase the risk for sporadic PD (Fuchs et al., 2009; Haubenberger et al., 2011). The polymorphism is in a non-coding region of the gene and thus might "solely" decrease the expression of *EN1* rather than disrupting gene function. A situation that is modeled in the heterozygous *En1* ko mice. In this line, conditional ablation of Nato3 in dopaminergic neurons leads to a significant reduction of En1 expression, mitochondrial dysfunction, and PD-like behavioral phenotypes (Miozzo et al., 2022). However, even though there are several hints that En1 acts neuroprotective in adult DAns, the analysis of En1 function in adults is hampered by the severe developmental phenotype of homozygous *En1* ko mice leading to their perinatal death (Wurst et al., 1994). Furthermore, even though the En1 function has been addressed intensively in animal models, to our knowledge no human model exists so far to translate the major findings in mouse into a human setting. To do so, we generated *EN1* deficient hiPSC derived neural precursor cells and neuronal cultures differentiated by a protocol inducing neurons with ventral midbrain identity identity which both represent a developmental and mature state, respectively.

The *EN1* knock-out was achieved by the introduction of indels into exon 1 of the *EN1* locus using the CRISPR/Cas9 system. This resulted in premature stop codons and termination of translation at around bp 430 downstream of the transcription start site. Regarding the structure of *EN1*, this refers to a region located shortly behind the EH1 domain (Logan et al., 1992), meaning that the EH1 and the eIF4E binding sites were still transcribed. However, as the premature termination occurs more than 50-55 bp upstream of the exon-exon junction in the hiPSCs, the truncated *EN1* mRNA is subjected to nonsense-mediated mRNA decay following the 50-55 nucleotide rule (Lykke-Andersen and Jensen, 2015; Nagy and Maquat, 1998). Once in the cytoplasm, mRNAs are subjected to nonsense-mediated mRNA decay within a minute (Trcek et al., 2013). Therefore, translation of the N-terminal part of *EN1* is highly unlikely. Due to missing functional antibodies, validation of the knock-out on protein level was unsuccessful using western blot and immunohistochemistry. Nevertheless, the RT-qPCR and the transcriptome analysis in which the clones were separated according to their genotype proved the successful *EN1* knock-out generation.

Concerning the functional analysis of this human cellular model the focus was set on mitochondrial dysfunction since it has already been linked to En1 in mice (Rekaik et al., 2015) and is one of the major culprits in PD etiology (Exner et al., 2012). En1 – as a translational regulator – has been shown to stimulate the translation of nuclear-encoded mitochondrial mRNAs for Ndufs1/Ndufs3, thereby influencing complex I activity and as a consequence ATP production (Alvarez-Fischer et al., 2011). In contrast, in the EN1 deficient human

neural precursor cells neither complex I activity nor the abundance of the respiratory complexes or cellular respiration per se were changed. However, these cells express *EN1* at a very low level implicating that EN1 function is not yet relevant for mitochondrial function at this early developmental stage.

When differentiating the precursor cells further into neurons with ventral midbrain identity i.e. TH+ neurons, it is surprising that EN1 deficiency does not influence differentiation efficiency, even though EN1 is instrumental in this process at very early stages (Alves dos Santos and Smidt, 2011). It is known from mice that En2 – which is still expressed in the *EN1* ko lines – can compensate for En1 function during early development (Albéri et al., 2004; Hanks et al., 1995; Simon et al., 2001). However, it might not be able to compensate for later developmental processes. Indeed, EN1 deficiency has an impact on neurite length in neurons. This might be due to an effect on neurite outgrowth per se during early differentiation or due to degenerative processes in developed neurons. It is tempting to speculate that this phenotype might be due to En1's non-cell-autonomous neurotrophic activity (Lebœuf et al., 2023). En1 stimulates axon growth (Brunet et al., 2005; Wizenmann et al., 2009) likely by the activation of axonal translation of e.g. mitochondrial complex I proteins. Thereby it concomitantly also increases ATP levels (Stettler et al., 2012). This is in line with young *EN1* deficient neurons exhibiting mitochondrial dysfunction with reduced levels of complex I. Also, the current transcriptome analysis supports this notion, since in both experimental paradigms - untreated and Wnt-stimulated hNPCs - mitochondrial genes and pathways are not dysregulated, even though in Wnt-stimulated hNPCs a clear mitochondrial dysfunction is obvious. Thus, during differentiation, EN1 might act mainly as non-cell-autonomous neurotrophin and the reduced neurite length might be caused by energy failure in the distal ends of neurites as it has been proposed in En1 heterozygous mice (Lebœuf et al., 2023; Nordströma et al., 2015). In sum, these findings indicate that EN1-deficiency in a human cellular model system exhibits similar phenotypes as the En1 heterozygous mouse model.

A totally new and unexpected finding was the involvement of EN1 in PC morphology and possibly function. Even if it is tempting to assume that EN1 could directly intervene in the molecular mechanisms responsible for PC morphology and thus PC function based on the transcriptome data presented, caution is advised. PC morphology and function is highly dynamic and depends on many distinct cellular processes, such as the mitotic state of cells, confluency of the culture, clonal effects, or even mitochondrial function. While we cannot exclude an effect of the mitotic state of hNPCs, we controlled for confluency, eliminated clonal effects by using multiple clones for each line, and showed that mitochondrial function is not altered in unstimulated *EN1* ko hNPCs. Thus, it is highly likely that EN1 indeed affects PC morphology and function. However, where EN1 might interfere with PC biology has still to be determined.

An equilibrium of assembly and disassembly is thought to maintain an appropriate ciliary length. As cilia typically lack the machinery that is necessary for protein synthesis, they rely on intracellular and intraflagellar transport (IFT) systems for the delivery of new building blocks such as tubulins to their site of assembly (Rosenbaum and Witman, 2002). The cargo molecules that accumulate at the ciliary base are bound by IFT-B complexes which, together with Kinesin-II family motors, mediate their anterograde transport towards the ciliary tip. The retrograde transport in contrast is mediated by dynein-II and IFT-A complexes (Ishikawa and Marshall, 2017; Prevo et al., 2017; Rosenbaum and Witman, 2002). Together they determine the concentration of proteins within PC and thus PC morphology and functionality.

Based on the transcriptome data, mainly one process might be responsible for the observed alterations in PC, namely the retrograde transport system. Various components of the dynein-2 and the IFT-A complexes were dysregulated in *EN1* ko cells, among them the core motor subunit DYNC2H1 of the dynein-2 complex (Vuolo et al., 2020) which was downregulated by ~30 %. Additionally, also one of the core subunits of the IFT-A complex namely IFT122 was downregulated in the *EN1* ko cells to a similar extent as the core motor subunit DYNC2H1. In line with this, also the CPLANE complex was heavily affected in *EN1* ko cells. The CPLANE complex consists mainly of the 5 subunits CPLANE1, INTU, WDPCP, CPLANE2, and FUZ with the first two being downregulated and the last two being upregulated in *EN1* ko cells. The precise function of the CPLANE complex during ciliogenesis and PC maintenance remains largely elusive, however, it has been related to proper IFT-A function (Martín-Salazar and Valverde, 2022). In the absence of the CPLANE complex, peripheral IFT-A components fail to localize to basal bodies and are thus not integrated together with the core IFT-A components into functional IFT-A complexes. A dysfunctional retrograde IFT system likely causes the over-accumulation of e.g. membrane proteins which is a known driver of cilia extension (Hesketh et al., 2022).

Functionally, this might impact the ability of cells to appropriately transduce signaling events that rely on PC, such as SHH or Wnt signaling. The PC is thought to control the expression of Wnt target genes through the controlled degradation of Dvl by ciliary proteins, and by sequestering AHI1 so that it cannot support the translocation of β-catenin into the nucleus (Wheway et al., 2018). Furthermore, the depletion of PC increased canonical Wnt signaling, which confirms an inhibitory role of PC on Wnt/β-catenin signaling (Lee, 2020). Similarly, the EN1-mediated PC deficiency seemed to result in the overactivation of the Wnt signaling pathway in our *EN1* ko hNPCs, resulting in a reduction in ciliogenesis and elongation in ciliary length. This is consistent with Wnt/ß-catenin signaling not being involved in cilia formation but rather having a suppressive effect. This has also been observed in mice neural progenitor cells of the developing cerebral cortex where activation of the Wnt/β-catenin pathway impeded ciliogenesis (Nakagawa et al., 2017).

As the Wnt stimulated *EN1* ko cells failed to convey the "normal" effect of Wnt signaling on mitochondrial and ciliary functions, it can be hypothesized that EN1 is an essential mediator of Wnt-induced adaptations. This might be mediated through the enhanced translation of target transcripts to increase mitochondrial respiration or by providing correct PC functionality that is essential to fine-tune Wnt signal transduction.

Interestingly, PC are receiving increasing attention as a critical factor linked to the vulnerability of DAns in PD. In many cases, also dysfunctional IFT seems to underlie the PC deficiencies. For example, a single-cell transcriptome analysis of neuronal cells differentiated from hiPSC from sporadic PD patients highlights the relevance of the IFT together with the BBSome for the onset of PD (Schmidt et al., 2022a). This notion is supported by a recent transcriptome analysis of postmortem tissue (Donega et al., 2019; Laperle et al., 2020) and a meta-analysis of sporadic PD patient tissue (Wang et al., 2019). Additionally, the hiPSC-derived hNPCs and DAns exhibited reduced mitochondrial respiration as part of a general hypometabolism (Schmidt et al., 2023). These metabolic alterations were introduced by alterations in SHH signal transduction which is mediated by PC. Interestingly, also genes associated with familial PD such as *LRRK2* or *PINK1* have been linked to PC formation recently. Alterations in PC morphology were observed in both human and mouse models with *PINK1* mutations (Schmidt et al., 2022a). Furthermore, PINK1 has already been associated with dysfunctional intracellular transport mechanisms, some of which overlap with the IFT system (Das Banerjee et al., 2017). Besides, also *Lrrk2* mutations have been associated with a loss of cilia in vitro and in vivo via altered RAB phosphorylation (Dhekne et al., 2018; Sobu et al., 2021). These implications of familial PD-associated genes on PC formation seem to be independent of their well-known involvement in mitochondrial quality control.

Both Wnt and SHH signaling which rely on PC for signal transduction are crucial for midbrain specification, DAn differentiation, but also maintenance (Kim et al., 2021; Kim et al., 2018). That midbrain markers such as EN1 might interfere with PC functionality and thus signal

transduction of e.g. Wnt signaling, highlights PC as a contributing factor to the specific vulnerability of midbrain DAns in PD.

All in all, the protective effect of EN1 for ventral midbrain neurons – including DAns - appears to be largely conserved between mouse and human rendering it a potential therapeutic option to halt the progression of PD. Indeed, EN1 has already been shown to induce long-lasting behavior benefits in an experimental Parkinson's disease primate model (Thomasson et al., 2019). In parts, EN1 seems to fulfill this function by fine-tuning Wnt signal transduction via PC. This further strengthens the assumption that PC are crucial not only for ventral midbrain neuronal differentiation but also for the maintenance of neurons. If dysfunctional, the function of neurons to perceive their environment and adjust their functions accordingly is disturbed, rendering them vulnerable to neurodegeneration.

4. Methods

4.1. Ethical compliance

Work with human hiPSCs for non-commercial research was approved by the Ethics Committee of the Technical University Munich (219/20 S, 290/20 S). All related experiments and methods were performed in accordance with relevant guidelines and regulations. The HMGUi001-A hiPSC line (https://hpscreg.eu/cell-line/HMGUi001-A) was generated and characterized by Xianming Wang (Wang et al., 2018). The CRISPR-Cas9 induced *EN1* knock-out lines and respective controls were established and characterized as described in this work. To exchange selected *EN1* knock-out lines for research purposes the Institute of Developmental Genetics will consider each request.

4.2. Cultivation of human cell lines

HEK293 cells were cultivated in a growth medium (Advanced DMEM supplemented with GlutaMAX and 10% FCS) (Thermo Fisher Scientific, 12491023) at 37°C and 5 % CO_2 with medium change every other day. When cells reached a confluency of about 90% cells were passaged at a dilution of 1:10.

4.3. Cultivation of hiPSCs

hiPSCs were cultivated in Essential 8 (E8) Flex Medium (Thermo Fisher Scientific, A2858501) under feeder-free conditions on Geltrex-coated plates (Thermo Fisher Scientific, A1413302) at 37°C, 5 % CO2, and 21% O_2. When cells reached a confluency of 70%, colonies were detached by adding StemMACS Passaging Solution XF (Miltenyi Biotec, 130-104-688) and incubation for 5 min at 37°C. The Passaging solution was aspirated, and colonies were chopped in 1 ml E8 Flex Medium using a 1000 µl pipette tip. hiPSCs were diluted and seeded at the desired density on fresh Geltrex-coated plates.

4.4. Differentiation and cultivation of hNPCs

hiPSCs were differentiated into small molecule neuronal progenitor cells (hNPCs) via an embryoid body stage according to the protocol described (Reinhardt et al., 2013) with minor adaptations. When hiPSCs reached a confluency of approximately 70%, colonies were detached using collagenase type IV (2 mg/ml) (Thermo Fisher Scientific, 17104019) and incubation for 40-60 min at 37°C, 5% CO_2, 21%O_2. The detached colonies were resuspended in KnockOut-Serum Replacement Medium (80% KnockOut DMEM (Life Technologies, 10829018) supplemented with 20% Knockout serum replacement (Life Technologies, 10828028), 10 µM SB431542 (Miltenyi Biotec, 130-106-275), 1 µM dorsomorphin (Tocris Bioscience, 3093/10), 0.5 µM purmorphamine (Tocris Bioscience, 4551), 4.44 nM FGF-8b (Miltenyi Biotec, 130-095-741), 3 µM CHIR99021 (Tocris Bioscience, 4423/10), 1% non-essential amino acids (Life Technologies, 11140035), 1% L-glutamine (Life Technologies, 5030024), 150 µM ascorbic acid 2-phosphate (Sigma, A8960-5G) and 0.02% beta-mercaptoethanol (Life Technologies, 31350010)). The colonies were cultivated for two days in a non-coated 6-well plate on a shaker at 37°C, 5% CO_2, and 21%O_2 at 80 rpm with daily medium changes. On day 3, the EBs were changed to neuronal precursor medium (50% DMEM/F12-GlutaMAX (Life Technologies, 31331093), 50% Neurobasal (Life Technologies, 21103049) supplemented with 1% B27 minus vitamin A (Life Technologies, 12587010), 0.5% N2 (Life Technologies, 17502048), 10 µM SB431542, 1 µM dorsomorphin, 0.5 µM purmorphamine, 4.44 nM FGF-8b, 3 µM CHIR99021, 150 µM ascorbic acid 2-phosphate and 0.02 % beta-mercaptoethanol) and maintained in this medium for 4 days on a shaker at 80 rpm at 37°C, 5% CO_2, 21%O_2 with daily medium changes. The EBs were transferred to neuronal precursor maintenance medium (neuronal precursor medium without purmorphamine and CHIR99021) at day 6 and seeded on Geltrex-coated plates the following day. hNPCs were expanded for 3-4 days in neuronal precursor maintenance medium with daily medium change. We termed these hNPCs "primed" for ventral midbrain identity since they were already grown in the presence of FGF8. When hNPCs were confluent after 10-11 days, cells were detached using Accutase (Sigma, A6964-500ML) for 10 min at 37°C, 5% CO_2, 21% O_2. Using a 1000 µl pipette tip, cells were harvested and transferred into a falcon tube containing 5 ml neuronal precursor maintenance medium. The cells were pelleted by centrifugation for 5 min at 200 g, resuspended in fresh neuronal precursor maintenance medium, and seeded on Geltrex-coated plates. From this point on, hNPCs were cultivated at 37°C, 5% CO_2, 21%O_2, and passaged at 80 % confluency using accutase. The medium was changed daily.

4.5. Differentiation into human dopaminergic neurons

hNPCs were differentiated into TH+ neurons following the protocol described by (Reinhardt et al., 2013). The differentiation was performed on poly-L-ornithine (Sigma, P3655) and laminin (Thermo Fisher Scientific, 23017015) coated plates. The following growth factors were used for the differentiation: 10 ng/mL human GDNF (Miltenyi Biotec, 130-096-291); 10 ng/mL human BDNF (Miltenyi Biotec, 130-093-811); 100 ng/mL human FGF-8b; 1 ng/mL human Tgf-beta3 (Miltenyi Biotec, 130-094-008); 200 µM ascorbic acid 2-phosphate; 1 µM purmorphamine; 500 µM dbcAMP (Sigma, D0627-1G). TH+ cells were differentiated for at least 42 days starting from initiation at 37°C, 5% CO_2, 21%O_2 with medium changes every 3-5 days.

4.6. Generation of EN1 knock-out hiPSC clones and quality control

The guide RNAs (gRNA) targeting the beginning of Exon 1 of the human *EN1* gene (5'-AGTTGGTGGTGCGGTGCAGC-3') was designed using the online tool CRISPOR (http://crispor.tefor.net/) and cloned into the pU6-(BbsI)sgRNA_CAG-Cas9-venus-bpA plasmid using a BbsI (New England Biolabs, R0539) restriction digest. The HMGUi001-A hiPSC line was transfected with the pU6-(BbsI) sgRNA_CAG-Cas9-venus-bpA plasmid and a plasmid encoding the anti-apoptotic protein BCL-XL (equal ratio, 2,5 µg DNA/6-well). The cells were seeded using Accutase one day prior to transfection (passage 28) at a density of 4 x 105 cells per 6-well in E8 Flex Medium containing 10 µM ROCK inhibitor Y27632 (Enzo Life Science, ALX-270333-M005). ROCK inhibitor Y27632 was removed 4 h before the transfection using Lipofectamine Stem Transfection Reagent (Thermo Fisher Scientific, STEM00001) according to the protocol with 20 min of incubation at RT. Medium was changed the next day and cells were sorted 48 h after transfection for reporter-positive cells. For the sorting, the cells were detached using Accutase, resuspended in E8 Flex medium containing 10 µM ROCK inhibitor Y27632, and put through a cell strainer before proceeding to the fluorescent activated cell sorting. Reporter-positive hiPSCs were plated at a low density (~2000 cells) on a 10 cm dish in E8 Flex Medium containing 10 µM ROCK inhibitor Y27632 and Penicillin/Streptomycin

(1:100) (Thermo Fisher Scientific, 15140122). After two days, the medium was changed to E8 Flex containing CloneR supplement (1:10) (Stemcell Technologies, 05888). After 4 days the medium was changed to E8 Flex. Once they reached a sufficient size, colonies were manually picked, chopped 2-3 times with the 1000 µl pipette tip, and replated on a Geltrex-coated 24-well plate in E8 Medium containing 10 µM ROCK inhibitor Y27632 for 1 day, before changing to E8 Medium. The colonies were characterized by sequencing of the genomic DNA (QIAamp DNA Mini Kit, Qiagen, 51306) of the targeted region of the *EN1* locus (hEN1_Exon1_fwd CTCACAGACCCATAATCCTG, hEN1_Exon1_rev TTGGCTGAGCCCATAAGTAG. To generate corresponding wildtype (WT) control clones, HMGUi001-A cells were seeded at a low density to allow the picking of single clones and processed similarly to the manipulated cells.

Selected knock-out and WT clones were re-clonalized. Cells were detached using Accutase, resuspended in E8 Flex Medium containing CloneR (1:10), and passed through a cell strainer. The cells were diluted to a concentration of 0.8 cells per 100 µl in E8 Flex medium containing CloneR and plated on a Geltrex-coated 96-well plate using 100 µl per well. Medium was changed after 2 days and after 4 days medium was changed back to E8 Flex without CloneR. Once colonies had a sufficient size, the hiPSCs were transferred to a coated 24-well plate using a passaging solution. For further characterization, subcloning of the *EN1* cDNA was performed using the TOPO™ TA Cloning™ Kit for Sequencing according to the manufacturer's instructions (hEN1_cDNA_fwd ATGGAAGAACAGCAGCCGG and hEN1_cDNA_rev CCTACTCGCTCTCGTCTTTGT) and plasmids were sequenced. Correct clones and selected WT clones (P42-45) were screened for Copy number variations (CNVs) using the HumanCytoSNP-12 BeadChip (knock-outs) (Illumina) and the Infinium Global Screening Array-24 v3.0 Kit (WT's) (Illumina). Downstream analysis including clustering, quality control, and SNP calling was performed using Genome Studio 2.0 (Illumina) as described by (Guo et al., 2014). CNVs for each cell clone were determined using the B-allele frequency (BAF) and log2 R ratios with the cnvPartition v3.2.1 plug-in (Illumina). cnvPartition v3.2.1 was run with default settings and a confidence threshold of 50. CNVs greater than 100 kb were considered. Trilineage differentiation was performed using the STEMdiff Trilineage Differentiation Kit (Stemcell Technologies, 05230) according to the manufacturer's instructions.

4.7. Protein isolation and immunoblotting

For protein isolation, cells were lysed in RIPA buffer (50 mM Tris-HCL (Sigma, T3253), 150 mM NaCl (Merck, 106404), 1% Triton X-100, 0.5% sodium deoxycholate (Sigma, D6750), 0.1% SDS (Sigma, L3771), 3 mM EDTA (Sigma, EDS-1KG)) supplemented with protease inhibitors (Roche Diagnostics, 11836170001) and collected using a cell scraper. After incubation on ice for 10 min, cell debris was removed by centrifugation at 21000g, 4 °C for 15 min. Proteins were stored in aliquots at -80°C or used directly (complex I activity assay). The protein concentration was determined using a Pierce BCA assay kit (Thermo Fisher Scientific, 23225) according to the manufacturer's instructions.

For quantification, proteins were thawed on ice, diluted to the desired concentration (5 µg) with RIPA buffer and NuPAGE™ LDS-sample buffer (Novex, NP0007), and heated for 5 min to 60°C. Proteins and Protein Marker VI (AppliChem, A8889) were separated on a Criterion XT 4-12% Bis-Tris Gel (Bio-Rad, 3450124) at 180 V for 75 min in 1x XT MOPS running buffer (Bio-Rad, 1610788) using a Criterion Vertical Electrophoresis Cell (BioRad). Proteins were blotted on an Immobilon-P membrane (Merck Millipore, IPVH00010) with a Criterion Blotter (Bio-Rad) using 1x Tris/Glycine buffer (Bio-Rad, 1610734) at 60 V for 2 h at 4°C. The membrane was blocked with 5 % milk (Sigma, 70166-500G) in TBS (Sigma, 93352) with 0.01 % Tween (TBS-T) (Sigma, P1379) for 75 min at room temperature. Primary antibodies anti-MTCO2 (Abcam, ab110258, 1:500), anti-NDUFB8 (Novex, 459210, 1:1,000), anti-Complex II subunit 30 (Thermo Fisher Scientific, 459230, 1:500), anti-ATP5A (Abcam, ab14748, 1:20,000), anti-NDUFS1 (Abcam, ab157221, 1:5,000), anti-NDUFS3 (Abcam, ab183733, 1:5,000), or anti-UQCRC2 (Abcam, ab14745, 1:2,500) in 5 % milk in TBS-T were incubated overnight at 4°C at 20 rpm. The membrane was washed three times for 15 min with TBS-T rotating at 15 rpm and the secondary antibody goat-anti-mouse IgG peroxidase (Dianova, 115-035-003, 1:10,000), or goat-anti-rabbit IgG peroxidase (Dianova, 111-035-003, 1:10,000) together with GAPDH coupled to a peroxidase (GeneTex, GTX627408, 1:10,000) (in 5 % milk in TBS-T) were added and incubated for 1 h. After three washing steps with TBS-T, the proteins were detected using Clarity Max ECL detection substrate (Bio-Rad, 1705062) and visualized using a Fusion SL Gel chemiluminescence documentation system (PEQLAB). Protein levels were quantified using Image Lab.

4.8. RNA isolation, cDNA synthesis, and quantitative real-time PCR (RT-qPCR)

RNA was isolated using the RNeasy Plus Mini Kit (Qiagen, 74134) according to the manufacturer's instructions. The RNA was reverse transcribed to cDNA using the VILO cDNA Synthesis kit (Thermo Fisher Scientific, 11754050). Gene expression was analyzed by RT-qPCR on a QuantStudio 7 Flex Real-Time PCR system (Thermo Fisher Scientific). 25 ng cDNA (2.78 ng/µl) was amplified using TaqMan universal PCR MM no UNG (Thermo Fisher Scientific, 4324018) or TaqMan Fast Advanced Master-Mix (Thermo Fisher Scientific, 4444556) and gene-specific TaqMan probes (Thermo Fisher Scientific, 4331182): ACTB (Hs99999903_m1), DLK1 (Hs00171584_m1), EN1 (Hs00154977_m1), EN2 (Hs00171321_m1), EPHA3 (Hs00739092_m1), HOXB9 (Hs00256886_m1), MAOA (Hs00165140_m1), OLIG2 (Hs00377820_m1), SLC16A3 (Hs00358829_m1), SP5 (Hs01370227_mH), SPARCL1 (Hs00949886_m1). The difference in gene expression was assessed by using the comparative Ct method and normalized to ACTB.

4.9. MitoTracker staining

hNPCs were seeded at a density of 20,000 cells per well and cultivated in their respective medium on 96-well plates. After 3 days, MitoTracker Orange CMTMRos (Thermo Fisher Scientific, M7510) was added at a final concentration of 100nM in a prewarmed medium, and cells were incubated for 20 min at 37°C, 5% CO_2, 21%O_2. Cells were washed with PBS twice and fixed with 10 % formalin (Sigma, F5554) for 15 min at RT. Fixed cells were washed three times with PBS and DAPI (Thermo Fisher Scientific, 62248) staining was performed. In the case of CHIR99021 stimulation, the neuronal precursor maintenance medium was supplemented with 3 µM CHIR99021 for 48 h before the MitoTracker staining with daily medium changes. The Cellinsight NXT platform with a 20x 0.4 NA objective (field size 454.41 by 454.41 µm) was used to acquire images for fluorescence intensity quantification and HCS Studio 2.0 was used for analysis. The configurations were adjusted for every antibody and chromophore. DAPI staining was performed to label all nuclei and the cytoplasmic MitoTracker intensity of all valid objects was detected in channel 2 using a fixed exposure time and a ring mask (RingSpotAvgIntenCh2). A distribution analysis was performed with 100 hNPCs per clone. In addition, the average fluorescence intensity per cell clone was quantified.

4.10. Respiratory and glycolytic flux analysis

Respiratory and glycolytic flux analysis was performed for hNPCs and neuronal cultures containing TH+ neurons.

hNPCs were maintained in neuronal precursor maintenance medium on Geltrex-coated plates at 37°C, 5% CO_2, 21%O_2. hNPCs were passaged at 80 % confluency. 70.000 cells per well were seeded on Geltrex-coated XF96 cell culture microplates (Agilent Technologies, 101085004) in neuronal precursor maintenance medium containing 10 µM ROCK

inhibitor Y27632. Cells were incubated for 72 h before Seahorse measurement with daily medium changes. After 24 h, the medium was changed to the neuronal precursor maintenance medium without ROCK inhibitor Y27632. At least 6 replicates per cell clone were seeded. For the CHIR99021 stimulation, hNPCs were seeded in the neuronal precursor maintenance medium containing 10 μM ROCK inhibitor Y27632. After 24 h, ROCK inhibitor Y27632 was removed and 3 μM CHIR99021 was added for 48 h with daily medium change.

For TH+ neurons, cells were passaged at day 9 of differentiation according to the protocol as described before. Neuronal cultures containing TH+ neurons were seeded in two different densities (2000 and 3000 cells per well) on poly-L-ornithine/laminin-coated XF96 cell culture microplates. Cells were allowed to mature until day 42 of the differentiation with medium changes every 2-5 days. At least 6 replicates per cell clone were seeded for each density.

The respiratory analysis was performed using a Seahorse XF96 Analyzer (Agilent Technologies). All measurements and dilutions were performed in XF Assay medium (Agilent Technologies, 103334-100). Prior to the Seahorse analysis, the cells were washed with XF Assay medium and incubated for 1 h at 37 °C, 0 % CO_2, 21 % O_2 in XF Assay medium supplemented either with 25 mM glucose (Thermo Fisher Scientific, 15023021) or 5 mM pyruvate (Sigma, P5280-25G). At least three replicates per substrate and cell clone were measured. The XFe96 Sensor Cartridges (Agilent Technologies, 102416100) were hydrated with 200 μl H_2O per well overnight and 200 μl calibrant for at least 1 h at 37 °C. The ports were loaded from A to D with 10 μg/ml oligomycin (Sigma, O4876-5MG), 5 μM FCCP (Sigma, C2920-10MG), 50 μM rotenone (Sigma, R8875-1G) with 20 μM antimycin A (Sigma, A8674-50MG) and 1 M 2-deoxyglucose (Sigma, D8375-25G).

After equilibration of the cartridge, basal respiration was assessed with four measurement points (mix for 1 min, 2 min time delay, measure for 3 min). The ports were then injected one after the other followed by three measurement points after each injection. Data visualization and exportation was performed using Wave 2.6.1. All data were normalized to DNA content, either quantified from the analyzed plate (same plate) (TH+ cells) or an equally seeded and grown copy plate (hNPCs). The DNA content was quantified using the Quant-iT PicoGreen dsDNA Assay Kit (Thermo Fisher Scientific, P11496). For copy plate analysis, cells were lysed in 60 μl RIPA buffer per well for 20 min on ice. In case the DNA was quantified from the same plate, 10 μl Proteinase K (20 mg/ml; AppliChem, A3830) were added per well, and cells were lysed at 37°C for 1 h. The plates were then centrifuged for 30 min or 5 min at 3000 g, respectively and the supernatant was used for DNA quantification. The Quant-iT PicoGreen dsDNA Assay was performed according to the manufacturer's instructions using Lambda DNA standards to calculate the DNA concentrations by linear regression. For statistical analysis, the mean oxygen consumption rate (OCR) values for basal (measuring points 1-4) and maximal mitochondrial (measuring points 8-10) respiration as well as for the proton leak (measuring points 5-7) were calculated for each clone. The OCR caused by non-mitochondrial respiration (measuring points 11-14) was subtracted from each value.

Basal glycolytic flux and glycolytic capacity were calculated from the mean extracellular acidification rate (ECAR) values from measuring points 1-4 and measuring points 5-7, respectively. The last measuring point represents the non-glycolytic acidification and was subtracted from all values.

4.11. Analysis of complex I activity

Complex I activity was analyzed using the Complex I Enzyme Activity Assay Kit (Abcam, ab109721) according to the manufacturer's instructions. Protein was isolated freshly, and a concentration of 1250 μg/ml was used in the assay. Kinetics were measured every 30 sec for 30 min on a SpectraMax M5 microplate (Molecular Devices) reader. The relative complex I activity is normalized to the complex I activity of WT clones.

4.12. Immunocytochemistry and imaging of human cells

For immunocytochemistry, cells were cultivated on coated glass coverslips or 96-well plates. Cells were washed with PBS and fixed with 10 % formalin for 15 min at RT. After three washing steps with PBS, cells were permeabilized and blocked with PBS containing 1 % Bovine Serum Albumin (BSA) (Sigma, A7906-500G) and 0.3 % Triton-X-100 (Sigma, T9284) for 15 min. Primary antibodies were diluted in 1% BSA and 0.3 % Triton-X-100 were added overnight at 4°C. Cells were washed three times with PBS before the secondary antibodies, diluted in 1 % BSA and 0.3 % Triton-X-100 were added for 1 h at RT in the dark. Next, the cells were washed twice with PBS, and nuclei were stained by adding DAPI-solution (100 ng/ml in PBS) for 5 min at RT. After two washing steps with PBS, coverslips were mounted using Aqua-Poly/Mount (Polysciences Inc., 18606-20). Primary antibodies: FOXA2 (R&D, AF2400, 1:200), NANOG (R&D Systems, AF1997, 1:200), NCAM1 (Abcam, ab7813, 1:200), NESTIN (Thermo Fisher Scientific, MA1-110, 1:250), PAX6 (BioLegend, 19013, 1:200), POU5F1 (Cell Signaling, 2840S, 1:500), RBFOX (Abcam, ab104224, 1:800), SOX1 (Abcam, ab87775, 1:500), SOX2 (Cell Signaling, 2748, 1:200), SOX17 (R&D, AF1924, 1:200), TBXT (Abcam, ab209665, 1:1000), TH (PelFreez, P40101, 1:600), ARL13B (17711-1-AP, Proteintech; 1:500). Secondary antibodies: donkey-anti-goat IgG Alexa 488 (Thermo Fisher Scientific, A11055, 1:500), donkey-anti-goat IgG Alexa 594 (Thermo Fisher Scientific, A11058, 1:500), donkey-anti-mouse IgG Alexa 488 (Thermo Fisher Scientific, A21202, 1:500), donkey-anti-mouse IgG Alexa 594 (Thermo Fisher Scientific, A21203, 1:500), donkey-anti-rabbit IgG Alexa 488 (Thermo Fisher Scientific, A21206, 1:500), donkey-anti-rabbit IgG Alexa 594 (Thermo Fisher Scientific, A21207, 1:500). Fluorescent images were acquired using the Axio Imager.M2 microscope (Zeiss) with a 20x or 40x objective or the Cellinsight NXT platform (Thermo Fisher Scientific).

4.13. Quantification of primary cilia

hNPCs were seeded on Geltrex-coated glass coverslips in 24-well plates at a density of 300,000 cells/well. After 3 days, hNPCs were fixed and stained (for ARL13B and NES) as described above. Image stacks were taken using a Leica SP8 laser scanning confocal microscope equipped with 488, 561, and 633 nm lasers and a 63× objective. z-stacks were collapsed to maximum intensity projections and primary cilia length was measured using ImageJ 1.53c. In total, n=50-80 cilia per clone were quantified from three independent hNPC differentiations. The numbers of primary cilia per image were divided by the numbers of DAPI-stained nuclei to obtain the fraction of ciliated cells. In total, ~500 cells were analyzed.

4.14. Neuron counting and neurite quantification

For the quantification of TH+ neurons, cells were passaged at day 9 of differentiation according to the protocol as described before. Cells were seeded in two different densities (500 and 1,000 cells per well) on poly-L-ornithine/laminin-coated 96-well plates. Cells were allowed to mature until day 42 of the differentiation with medium changes every 2-5 days. At least 6 replicates per cell clone were seeded for each density. After maturation, neurons were fixed and stained (for TH and RBFOX3) as described above. Analysis was performed as described by (Schmidt et al., 2022a) using a Cellinsight NXT platform with a 20 × 0.4 NA objective (field size of 454.41 by 454.41 μm) and HCS Studio 2.0 (Neuronal Profiling Bioapplication). In total, twenty-five imaging fields were collected per well. DAPI-stained nuclei were identified in channel 1 using size, shape, and intensity thresholds within the HCS Studio. RBFOX3 (NeuN) fluorescence intensities within the nuclear mask were quantified in channel 2, and the TH fluorescence intensities were quantified within a ring (thickness 20 pixels) around the nuclear mask in channel 3. Intensity thresholds were applied to specifically filter for cells

with a robust expression of RBFOX3 and TH. Cells were classified as neurons if they had a DAPI and RBFOX3 (NEUN) positive nucleus, as well as TH+ neurons if they had in addition a TH-positive soma.

For the quantification of neurite length, neurons were identified based on RBFOX3 staining as described above. The TH fluorescence intensity in channel 3 was used by the Neuronal Profiling Bioapplication of the HCS Studio to determine cellular area based on intensity thresholds. Based on additional size and shape thresholds, the cell soma around the nuclear mask was quantified and neurites originating from the cell soma were tracked allowing for minimal gaps (4 pixels). Only neurites longer than 10 μm were included in the analysis. To account for variabilities in cell densities, the total neurite length was normalized to the number of TH+ neurons per image.

4.15. Transcriptome library preparation and sequencing

Gene expression profiling was performed at the stage of hNPCs. All 5 WT lines and the 3 *EN1* ko lines were used. hNPCs were seeded at a density of 1,000,000 cells per well on Geltrex-coated 6-well plates containing neural precursor maintenance medium supplemented with 10 μM ROCK inhibitor Y27632 (Enzo Life Science, ALX-270333-M005). In total, 6 replicates per cell line were prepared and incubated at 37 °C, 7% CO_2, and 21% O_2. The next day, the medium was changed to neural precursor maintenance medium for 3 replicates and to neuronal precursor maintenance medium supplemented with 3 μM CHIR99021 (Tocris Bioscience, 4423/10) for the other 3 replicates. After 48h, the RNA was isolated using the RNeasy Plus Mini Kit (Qiagen, 74134) according to the manufacturer's instructions. RNA libraries for RNA-seq were prepared using the TruSeq Stranded mRNA kit (Illumina) following the manufacturer's protocols. In total, 48 libraries were prepared. Libraries were pooled and paired-end sequencing (100bp per read) was performed on a NovaSeq 6000 (Illumina) with an estimated read depth of 30,000,000 reads per sample. Sequencing was performed in the genome analysis center of Helmholtz Munich.

4.16. Sequencing data processing

RNA-seq data were analyzed using a local Galaxy v 22.05 instance. The quality of sequencing reads stored in FASTQ files was assessed using FastQC v0.72. Paired-end reads were trimmed, and short reads (<20 bp) were removed using Trimmomatic v0.38.1. RNA STAR Aligner v2.7.8a was used to align sequence reads to the human reference genome GRCh38. Alignment summary statistics were reported using samtools idxstats v2.0.3. Alignment quality was further assessed using RSeQC v1.1 and its provided annotation BED files for the human reference genome GRCh38. The number of reads mapped to each gene was extracted from the STAR aligner BAM output file using featureCounts v1.6.4 and gene annotations (release 32) obtained from GENCODE. Gene counts were converted to a matrix using Count matrix v0.0.3. Output results from FastQC, Trimmomatic, STAR aligner, samtools idxstats, featureCounts, and RSeQC were aggregated using MultiQC v1.9.

4.17. Dimensionality reduction and correlation

Further analysis was performed using R v4.3.1. In brief, PCA was performed using the prcomp function and visualized using the package ggbiplot v0.55 with probability ellipses (0.68 of normal probability). The Pearson correlation between samples was calculated using the cor function within R, and correlations were plotted in a heatmap using the pheatmap function of the R package pheatmap v1.0.12. Agglomerative hierarchical clustering by the hclust function (method = "complete") was applied to group samples.

4.18. Differential expression analysis

Hypothesis testing was performed using the package DESeq2 v1.40.2 and the design formula design = ~clone.n + clone.n:replicate + condition with condition being either WT or *EN1* ko, clone.n being a unique number per cell line per condition, and replicate indicating the different replicates per cell line (1, 2, or 3). For assessing the stimulation effect, the design formula design = ~clone.n + clone.n:replicate + stimulation with stimulation being either unstimulated or CHIR99021 stimulated. The p-values were adjusted for multiple testing within DESeq2 by Benjamini and Hochberg (Benjamini and Hochberg, 1995). Genes with a p-adjust-value (q-value) < 0.05 were considered significantly altered in *EN1* ko NPCs.

4.19. Visualization of DEGs

Based on the complete set of differentially expressed genes (DEGs) a volcano plot and heatmap was produced. For the volcano plot, log2(fold change) was plotted versus the -log10(p-adjust-value) on the x and y-axis, respectively. The Volcano plot was generated using the EnhancedVolcano function of the R package EnhancedVolcano v1.18.0 with p-adjust cutoff = 0.05 and fold change cutoff = 0.5. The heatmap was generated by using the pheatmap function of the R package pheatmap v1.0.12. Agglomerative hierarchical clustering by the hclust function (method = "complete") was applied to group samples or genes. Log2 (fold changes) of DEGs were scaled and represented as z-score.

4.20. Pathway enrichment analysis

DEGs were investigated for enrichment in GO, KEGG, and WikiPathway (WP) terms using the enrichGO, enrichKEGG, or enrichWP function of the R package clusterProfiler v 4.8.3 (one-sided hypergeometric test). Enrichment of Reactome terms was assessed using the enrichPathway function of the R package ReactomePA v 1.44.0 (one-sided1 hypergeometric test). p-values were adjusted for multiple testing by Benjamini and Hochberg (Benjamini and Hochberg, 1995). Enrichment maps were generated using the treeplot function of clusterProfiler.

4.21. Statistics and reproducibility

The sample size was not predetermined by statistical methods. If not indicated otherwise, statistical analysis was performed using GraphPad Prism 6 with mean values of three biological replicates for n = 3 *EN1* ko and n = 5 WT clones. Two group comparison was performed between *EN1* ko with WT cell clones using an unpaired, two-tailed t-test in case of normal distribution. In the case of non-Gaussian distribution, a two-tailed Man-Whitney-U test was applied. Treated vs. untreated groups were compared using two-way ANOVA and Sidak (stimulation) and Tukey's (genotype) post-hoc tests. Boxplots are displayed with the box extending from the 25th to 75th percentile showing the median and whiskers ranging from min to max value with all data points shown.

If not stated otherwise, R version 4.3.1 and RStudio 2023.09.0 Build 463 was used for further analysis. Density plots or violin plots were used to visualize the distributions of repeated measurements per individual cell line (e.g. if multiple cells per cell line were analyzed). Density plots were generated using the function sm.density.compare of the R package sm v 2.2-5.7. Violin plots were generated using the functions ggplot + geom_violin of the R package ggplot2 v3.4.3. For the statistical analysis, a linear mixed effects model (lm) was fit using the lmer function (R package lme4 Version 1.1-31), where unique cells were included but nested within donors (formula: Parameter measured per cell ~ disease state + 1 | disease state:Patients; REML = FALSE). P values for lm were calculated using the Anova function (R package car Version 3.0-10). Boxplots summarizing measurements per individual cell line were generated using the functions ggplot + geom_boxplot of the R package ggplot2 v3.4.3. These boxplots display the median and range from the

25th to 75th percentile. Whiskers extend to the most extreme data point which is no more than 1.5 times the interquartile range.

If not stated otherwise, p-values or q-values below 0.05 were considered significant. Differences with a p-value or q-value between 0.05 and 0.1 were considered as trends (#). Not-significant differences are not indicated.

Supplementary data to this article can be found online at https://doi.org/10.1016/j.nbd.2024.106474.

CRediT authorship contribution statement

Sina Hembach: Writing – original draft, Methodology, Investigation, Formal analysis, Data curation, Conceptualization. **Sebastian Schmidt:** Writing – original draft, Visualization, Validation, Methodology, Investigation, Formal analysis, Data curation. **Tanja Orschmann:** Methodology, Investigation. **Ingo Burtscher:** Methodology, Investigation, Conceptualization. **Heiko Lickert:** Methodology, Investigation, Conceptualization. **Florian Giesert:** Writing – original draft, Supervision, Project administration, Investigation, Funding acquisition, Conceptualization. **Daniela Vogt Weisenhorn:** Writing – original draft, Supervision, Project administration, Investigation, Funding acquisition, Conceptualization. **Wolfgang Wurst:** Writing – original draft, Supervision, Project administration, Investigation, Funding acquisition, Conceptualization.

Declaration of competing interest

The authors declare no competing interests.

Data availability

Further information and requests for resources and reagents should be directed to and will be fulfilled by the corresponding author. The transcriptome data have been deposited to the NCBI Gene Expression Omnibus (GEO) under accession number GEO: GSE244435. Following databases were used within this study: GO terms [https://geneontology.org/] (downloaded on 09.2023), KEGG pathways [https://www.genome.jp/kegg/pathway.html] (downloaded on 09.2023), WikiPathway pathways [https://www.wikipathways.org/index.php/WikiPathways] (downloaded on 09.2023), Reactome pathways [https://reactome.org/] (downloaded on 09.2023). Analysis code and data is freely available at Github [https://github.com/sebischmidt/Engrailed1-deficiency-induces-changes-in-ciliogenesis-during-human-neuronal-differentiation] and has been deposited in Zenodo (Schmidt, 2024).

Acknowledgments

We thank Annerose Kurz-Drexler, Tanja Orschmann, and Susanne Badeke for excellent technical assistance. Funding: This work was supported by the Federal Ministry of Education and Research (BMBF) and the Bavarian State Ministry of Science and the Arts within the initial phase of the German Center for Mental Health (Deutsches Zentrum für Psychische Gesundheit [DZPG] (grant: 01EE2303E) and by the Helmholtz Association “ExNet-0041-Phase2-3 (‘SyNergy-HMGU’)”.

References

Alavian, K.N., Jeddi, S., Naghipour, S.I., Nabili, P., Licznerski, P., Tierney, T.S., 2014. The lifelong maintenance of mesencephalic dopaminergic neurons by Nurr1 and engrailed. J. Biomed. Sci. 21, 1–8. https://doi.org/10.1186/1423-0127-21-27.

Albéri, L., Sgadò, P., Simon, H.H., 2004. Engrailed genes are cell-autonomously required to prevent apoptosis in mesencephalic dopaminergic neurons. Development (Cambridge, England) 131, 3229–3236. https://doi.org/10.1242/dev.01128.

Alvarez-Fischer, D., Fuchs, J., Castagner, F., Stettler, O., Massiani-Beaudoin, O., Moya, K. L., Bouillot, C., Oertel, W.H., Lombès, A., Faigle, W., Joshi, R.L., Hartmann, A., Prochiantz, A., 2011. Engrailed protects mouse midbrain dopaminergic neurons against mitochondrial complex I insults. Nat. Neurosci. 14, 1260–1266. https://doi.org/10.1038/nn.2916.

Alves dos Santos, M.T.M., Smidt, M.P., 2011. En1 and Wnt signaling in midbrain dopaminergic neuronal development. Neural Dev. 6, 23. https://doi.org/10.1186/1749-8104-6-23.

Benjamini, Y., Hochberg, Y., 1995. Controlling the False Discovery Rate: A Practical and Powerful Approach to Multiple Testing. J. R. Stat. Soc. Ser. B Methodol. 57, 289–300. https://doi.org/10.1111/j.2517-6161.1995.tb02031.x.

Brunet, I., Weinl, C., Piper, M., Trembleau, A., Volovitch, M., Harris, W., Prochiantz, A., Holt, C., 2005. The transcription factor Engrailed-2 guides retinal axons. Nature 438, 94–98. https://doi.org/10.1038/nature04110.

Casar Tena, T., Maerz, L.D., Szafranski, K., Groth, M., Blätte, T.J., Donow, C., Matysik, S., Walther, P., Jeggo, P.A., Burkhalter, M.D., Philipp, M., 2019. Resting cells rely on the DNA helicase component MCM2 to build cilia. Nucleic Acids Res. 47, 134–151. https://doi.org/10.1093/nar/gky945.

Danielian, P.S., McMahon, A.P., 1996. Engrailed-1 as a target of the Wnt-1 signalling pathway in vertebrate midbrain development. Nature 383, 332–334. https://doi.org/10.1038/383332a0.

D’Antonio, M., Benaglio, P., Jakubosky, D., Greenwald, W.W., Matsui, H., Donovan, M.K. R., Li, H., Smith, E.N., D’Antonio-Chronowska, A., Frazer, K.A., 2018. Insights into the Mutational Burden of Human Induced Pluripotent Stem Cells from an Integrative Multi-Omics Approach. Cell Rep. 24, 883–894. https://doi.org/10.1016/j.celrep.2018.06.091.

Das Banerjee, T., Dagda, R.Y., Dagda, M., Chu, C.T., Rice, M., Vazquez-Mayorga, E., Dagda, R.K., 2017. PINK1 regulates mitochondrial trafficking in dendrites of cortical neurons through mitochondrial PKA. J. Neurochem. 142, 545–559. https://doi.org/10.1111/jnc.14083.

Davis, C.A., Joyner, A.L., 1988. Expression patterns of the homeo box-containing genes En-1 and En-2 and the proto-oncogene int-1 diverge during mouse development. Genes Dev. 2, 1736–1744. https://doi.org/10.1101/gad.2.12b.1736.

Dhekne, H.S., Yanatori, I., Gomez, R.C., Tonelli, F., Diez, F., Schüle, B., Steger, M., Alessi, D.R., Pfeffer, S.R., 2018. A pathway for Parkinson’s Disease LRRK2 kinase to block primary cilia and Sonic hedgehog signaling in the brain. eLife 7. https://doi.org/10.7554/eLife.40202.

Di Nardo, A.A., Nedelec, S., Trembleau, A., Volovitch, M., Prochiantz, A., Montesinos, M. L., 2007. Dendritic localization and activity-dependent translation of Engrailed1 transcription factor. Mol. Cell. Neurosci. 35, 230–236. https://doi.org/10.1016/j.mcn.2007.02.015.

Donega, V., Burm, S.M., van Strien, M.E., van Bodegraven, E.J., Paliukhovich, I., Geut, H., van de Berg, W.D.J., Li, K.W., Smit, A.B., Basak, O., Hol, E.M., 2019. Transcriptome and proteome profiling of neural stem cells from the human subventricular zone in Parkinson’s disease. Acta Neuropathol. Communicat. 7, 84. https://doi.org/10.1186/s40478-019-0736-0.

Exner, N., Lutz, A.K., Haass, C., Winklhofer, K.F., 2012. Mitochondrial dysfunction in Parkinson’s disease: molecular mechanisms and pathophysiological consequences. EMBO J. 31, 3038–3062. https://doi.org/10.1038/emboj.2012.170.

Ferguson, R.L., Pascreau, G., Maller, J.L., 2010. The cyclin A centrosomal localization sequence recruits MCM5 and Orc1 to regulate centrosome reduplication. J. Cell Sci. 123, 2743–2749. https://doi.org/10.1242/jcs.073098.

Fuchs, J., Mueller, J.C., Lichtner, P., Schulte, C., Munz, M., Berg, D., Wüllner, U., Illig, T., Sharma, M., Gasser, T., 2009. The transcription factor PITX3 is associated with sporadic Parkinson’s disease. Neurobiol. Aging 30, 731–738. https://doi.org/10.1016/j.neurobiolaging.2007.08.014.

Fuchs, J., Stettler, O., Alvarez-Fischer, D., Prochiantz, A., Moya, K.L., Joshi, R.L., 2012. Engrailed signaling in axon guidance and neuron survival. Eur. J. Neurosci. 35, 1837–1845. https://doi.org/10.1111/j.1460-9568.2012.08139.x.

Giesert, F., Glasl, L., Zimprich, A., Ernst, L., Piccoli, G., Stautner, C., Zerle, J., Hölter, S. M., Vogt Weisenhorn, D.M., Wurst, W., 2017. The pathogenic LRRK2 R1441C mutation induces specific deficits modeling the prodromal phase of Parkinson’s disease in the mouse. Neurobiol. Dis. 105, 179–193. https://doi.org/10.1016/j.nbd.2017.05.013.

Giguère, N., Burke Nanni, S., Trudeau, L.-E., 2018. On Cell Loss and Selective Vulnerability of Neuronal Populations in Parkinson’s Disease. Front. Neurol. 9, 455. https://doi.org/10.3389/fneur.2018.00455.

Glasl, L., Kloos, K., Giesert, F., Roethig, A., Di Benedetto, B., Kühn, R., Zhang, J., Hafen, U., Zerle, J., Hofmann, A., de Angelis, M.H., Winklhofer, K.F., Hölter, S.M., Vogt Weisenhorn, D.M., Wurst, W., 2012. Pink1-deficiency in mice impairs gait, olfaction and serotonergic innervation of the olfactory bulb. Exp. Neurol. 235, 214–227. https://doi.org/10.1016/j.expneurol.2012.01.002.

Goldberg, M.S., Pisani, A., Haburcak, M., Vortherms, T.A., Kitada, T., Costa, C., Tong, Y., Martella, G., Tscherter, A., Martins, A., Bernardi, G., Roth, B.L., Pothos, E.N., Calabresi, P., Shen, J., 2005. Nigrostriatal dopaminergic deficits and hypokinesia caused by inactivation of the familial Parkinsonism-linked gene DJ-1. Neuron 45, 489–496. https://doi.org/10.1016/j.neuron.2005.01.041.

Guo, Y., He, J., Zhao, S., Wu, H., Zhong, X., Sheng, Q., Samuels, D.C., Shyr, Y., Long, J., 2014. Illumina human exome genotyping array clustering and quality control. Nat. Protoc. 9, 2643–2662. https://doi.org/10.1038/nprot.2014.174.

Hanks, M., Wurst, W., Anson-Cartwright, L., Auerbach, A.B., Joyner, A.L., 1995. Rescue of the En-1 mutant phenotype by replacement of En-1 with En-2. Science 269, 679–682. https://doi.org/10.1126/science.7624797.

Haubenberger, D., Reinthaler, E., Mueller, J.C., Pirker, W., Katzenschlager, R., Froehlich, R., Bruecke, T., Daniel, G., Auff, E., Zimprich, A., 2011. Association of transcription factor polymorphisms PITX3 and EN1 with Parkinson’s disease. Neurobiol. Aging 32, 302–307. https://doi.org/10.1016/j.neurobiolaging.2009.02.015.

Hesketh, S.J., Mukhopadhyay, A.G., Nakamura, D., Toropova, K., Roberts, A.J., 2022. IFT-A structure reveals carriages for membrane protein transport into cilia. Cell 185, 4971–4985.e16. https://doi.org/10.1016/j.cell.2022.11.010.

Ishikawa, H., Marshall, W.F., 2017. Intraflagellar transport and ciliary dynamics. In: Cold Spring Harbor Perspectives in Biology, 9. https://doi.org/10.1101/cshperspect.a021998.

Kim, J.Y., Lee, J.S., Hwang, H.S., Lee, D.R., Park, C.-Y., Jung, S.J., You, Y.R., Kim, D.-S., Kim, D.-W., 2018. Wnt signal activation induces midbrain specification through direct binding of the beta-catenin/TCF4 complex to the EN1 promoter in human pluripotent stem cells. Exp. Mol. Med. 50, 1–13. https://doi.org/10.1038/s12276-018-0044-y.

Kim, T.W., Piao, J., Koo, S.Y., Kriks, S., Chung, S.Y., Betel, D., Socci, N.D., Choi, S.J., Zabierowski, S., Dubose, B.N., Hill, E.J., Mosharov, E.V., Irion, S., Tomishima, M.J., Tabar, V., Studer, L., 2021. Biphasic Activation of WNT Signaling Facilitates the Derivation of Midbrain Dopamine Neurons from hESCs for Translational Use. Cell Stem Cell 28, 343–355.e5. https://doi.org/10.1016/j.stem.2021.01.005.

Kyun, M.-L., Kim, S.-O., Lee, H.G., Hwang, J.-A., Hwang, J., Soung, N.-K., Cha-Molstad, H., Lee, S., Kwon, Y.T., Kim, B.Y., Lee, K.H., 2020. Wnt3a Stimulation Promotes Primary Ciliogenesis through β-Catenin Phosphorylation-Induced Reorganization of Centriolar Satellites. Cell Rep. 30, 1447–1462.e5. https://doi.org/10.1016/j.celrep.2020.01.019.

Laperle, A.H., Sances, S., Yucer, N., Dardov, V.J., Garcia, V.J., Ho, R., Fulton, A.N., Jones, M.R., Roxas, K.M., Avalos, P., West, D., Banuelos, M.G., Shu, Z., Murali, R., Maidment, N.T., van Eyk, J.E., Tagliati, M., Svendsen, C.N., 2020. iPSC modeling of young-onset Parkinson's disease reveals a molecular signature of disease and novel therapeutic candidates. Nat. Med. 26, 289–299. https://doi.org/10.1038/s41591-019-0739-1.

Lebœuf, M., Vargas-Abonce, S.E., Pezé-Hedsieck, E., Dupont, E., Jimenez-Alonso, L., Moya, K.L., Prochiantz, A., 2023. ENGRAILED-1 transcription factor has a paracrine neurotrophic activity on adult spinal α-motoneurons. EMBO Rep. 24, e56525 https://doi.org/10.15252/embr.202256525.

Lee, K.H., 2020. Involvement of Wnt signaling in primary cilia assembly and disassembly. FEBS J. 287, 5027–5038. https://doi.org/10.1111/febs.15579.

Liu, A., Joyner, A.L., 2001. EN and GBX2 play essential roles downstream of FGF8 in patterning the mouse mid/hindbrain region. Development (Cambridge, England) 128, 181–191. https://doi.org/10.1242/dev.128.2.181.

Logan, C., Hanks, M.C., Noble-Topham, S., Nallainathan, D., Provart, N.J., Joyner, A.L., 1992. Cloning and sequence comparison of the mouse, human, and chicken engrailed genes reveal potential functional domains and regulatory regions. Dev. Genet. 13, 345–358. https://doi.org/10.1002/dvg.1020130505.

Lykke-Andersen, S., Jensen, T.H., 2015. Nonsense-mediated mRNA decay: an intricate machinery that shapes transcriptomes. Nature reviews. Nat. Rev. Mol. Cell Biol. 16, 665–677. https://doi.org/10.1038/nrm4063.

Marie, B., Bacon, J.P., Blagburn, J.M., 2000. Double-stranded RNA interference shows that Engrailed controls the synaptic specificity of identified sensory neurons. Curr. Biol. 10, 289–292. https://doi.org/10.1016/S0960-9822(00)00361-4.

Martin, L.J., Pan, Y., Price, A.C., Sterling, W., Copeland, N.G., Jenkins, N.A., Price, D.L., Lee, M.K., 2006. Parkinson's Disease α-Synuclein Transgenic Mice Develop Neuronal Mitochondrial Degeneration and Cell Death. J. Neurosci. 26, 41–50. https://doi.org/10.1523/JNEUROSCI.4308-05.2006.

Martín-Salazar, J.E., Valverde, D., 2022. CPLANE Complex and Ciliopathies. Biomolecules 12. https://doi.org/10.3390/biom12060847.

McGrew, L.L., Takemaru, K., Bates, R., Moon, R.T., 1999. Direct regulation of the Xenopus engrailed-2 promoter by the Wnt signaling pathway, and a molecular screen for Wnt-responsive genes, confirm a role for Wnt signaling during neural patterning in Xenopus. Mech. Dev. 87, 21–32. https://doi.org/10.1016/s0925-4773(99)00136-7.

Miozzo, F., Valencia-Alarcón, E.P., Stickley, L., Majcin Dorcikova, M., Petrelli, F., Tas, D., Loncle, N., Nikonenko, I., Bou Dib, P., Nagoshi, E., 2022. Maintenance of mitochondrial integrity in midbrain dopaminergic neurons governed by a conserved developmental transcription factor. Nat. Commun. 13, 1426. https://doi.org/10.1038/s41467-022-29075-0.

Nagy, E., Maquat, L.E., 1998. A rule for termination-codon position within intron-containing genes: when nonsense affects RNA abundance. Trend Biochem. Sci. 23, 198–199. https://doi.org/10.1016/S0968-0004(98)01208-0.

Nakagawa, N., Li, J., Yabuno-Nakagawa, K., Eom, T.-Y., Cowles, M., Mapp, T., Taylor, R., Anton, E.S., 2017. APC sets the Wnt tone necessary for cerebral cortical progenitor development. Genes Dev. 31, 1679–1692. https://doi.org/10.1101/gad.302679.117.

Nédélec, S., Foucher, I., Brunet, I., Bouillot, C., Prochiantz, A., Trembleau, A., 2004. Emx2 homeodomain transcription factor interacts with eukaryotic translation initiation factor 4E (eIF4E) in the axons of olfactory sensory neurons. In: Proceedings of the National Academy of Sciences of the United States of America, 101, pp. 10815–10820. https://doi.org/10.1073/pnas.0403824101.

Nguyen, H.T., Geens, M., Mertzanidou, A., Jacobs, K., Heirman, C., Breckpot, K., Spits, C., 2014. Gain of 20q11.21 in human embryonic stem cells improves cell survival by increased expression of Bcl-xL. Mol. Hum. Reprod. 20, 168–177. https://doi.org/10.1093/molehr/gat077.

Nordströma, U., Beauvais, G., Ghosh, A., Pulikkaparambil Sasidharan, B.C., Lundblad, M., Fuchs, J., Joshi, R.L., Lipton, J.W., Roholt, A., Medicetty, S., Feinstein, T.N., Steiner, J.A., Escobar Galvis, M.L., Prochiantz, A., Brundin, P., 2015. Progressive nigrostriatal terminal dysfunction and degeneration in the engrailed1 heterozygous mouse model of Parkinson's disease. Neurobiol. Dis. 73, 70–82. https://doi.org/10.1016/j.nbd.2014.09.012.

Palacino, J.J., Sagi, D., Goldberg, M.S., Krauss, S., Motz, C., Wacker, M., Klose, J., Shen, J., 2004. Mitochondrial dysfunction and oxidative damage in parkin-deficient mice. J. Biol. Chem. 279, 18614–18622. https://doi.org/10.1074/jbc.M401135200.

Pézier, A., Jezzini, S.H., Marie, B., Blagburn, J.M., 2014. Engrailed alters the specificity of synaptic connections of Drosophila auditory neurons with the giant fiber. J. Neurosci. 34, 11691–11704. https://doi.org/10.1523/JNEUROSCI.1939-14.2014.

Poewe, W., Seppi, K., Tanner, C.M., Halliday, G.M., Brundin, P., Volkmann, J., Schrag, A.-E., Lang, A.E., 2017. Parkinson disease. Nature reviews. Disease Prim. 3, 17013. https://doi.org/10.1038/nrdp.2017.13.

Prevo, B., Scholey, J.M., Peterman, E.J., 2017. Intraflagellar transport: mechanisms of motor action, cooperation and cargo delivery. FEBS J. 284, 2905–2931. https://doi.org/10.1111/febs.14068.

Reinhardt, P., Glatza, M., Hemmer, K., Tsytsyura, Y., Thiel, C.S., Höing, S., Moritz, S., Parga, J.A., Wagner, L., Bruder, J.M., Wu, G., Schmid, B., Röpke, A., Klingauf, J., Schwamborn, J.C., Gasser, T., Schöler, H.R., Sterneckert, J., 2013. Derivation and expansion using only small molecules of human neural progenitors for neurodegenerative disease modeling. PLoS One 8, e59252. https://doi.org/10.1371/journal.pone.0059252.

Rekaik, H., Blaudin de Thé, F.-X., Prochiantz, A., Fuchs, J., Joshi, R.L., 2015. Dissecting the role of Engrailed in adult dopaminergic neurons–Insights into Parkinson disease pathogenesis. FEBS Lett. 589, 3786–3794. https://doi.org/10.1016/j.febslet.2015.10.002.

Rosenbaum, J.L., Witman, G.B., 2002. Intraflagellar transport. Nature reviews. Mol. Cell. Biol. 3, 813–825. https://doi.org/10.1038/nrm952.

Saueressig, H., Burrill, J., Goulding, M., 1999. Engrailed-1 and netrin-1 regulate axon pathfinding by association interneurons that project to motor neurons. Development (Cambridge, England) 126, 4201–4212. https://doi.org/10.1242/dev.126.19.4201.

Schmidt, S., 2024. sebischmidt/Engrailed1-Deficiency-Induces-Changes-in-Ciliogenesis-During-Human-Neuronal-Differentiation.. Publication release for Zenodo. https://doi.org/10.5281/zenodo.10812810.

Schmidt, S., Luecken, M.D., Trümbach, D., Hembach, S., Niedermeier, K.M., Wenck, N., Pflügler, K., Stautner, C., Böttcher, A., Lickert, H., Ramirez-Suastegui, C., Ahmad, R., Ziller, M.J., Fitzgerald, J.C., Ruf, V., van de Berg, W.D.J., Jonker, A.J., Gasser, T., Winner, B., Winkler, J., Vogt Weisenhorn, D.M., Giesert, F., Theis, F.J., Wurst, W., 2022a. Primary cilia and SHH signaling impairments in human and mouse models of Parkinson's disease. Nat. Commun. 13, 4819. https://doi.org/10.1038/s41467-022-32229-9.

Schmidt, S., Vogt Weisenhorn, D.M., Wurst, W., 2022b. Chapter 5 - "Parkinson's disease - A role of non-enzymatic posttranslational modifications in disease onset and progression?". Mol. Asp. Med. 86, 101096. https://doi.org/10.1016/j.mam.2022.101096.

Schmidt, S., Stautner, C., Vu, D.T., Heinz, A., Regensburger, M., Karayel, O., Trümbach, D., Artati, A., Kaltenhäuser, S., Nassef, M.Z., Hembach, S., Steinert, L., Winner, B., Jürgen, W., Jastroch, M., Luecken, M.D., Theis, F.J., Westmeyer, G.G., Adamski, J., Mann, M., Hiller, K., Giesert, F., Vogt Weisenhorn, D.M., Wurst, W., 2023. A reversible state of hypometabolism in a human cellular model of sporadic Parkinson's disease. Nat. Commun. 14, 7674. https://doi.org/10.1038/s41467-023-42862-7.

Seegobin, S.P., Heaton, G.R., Liang, D., Choi, I., Blanca Ramirez, M., Tang, B., Yue, Z., 2020. Progress in LRRK2-Associated Parkinson's Disease Animal Models. Front. Neurosci. 14, 674. https://doi.org/10.3389/fnins.2020.00674.

Sgadò, P., Albéri, L., Gherbassi, D., Galasso, S.L., Ramakers, G.M.J., Alavian, K.N., Smidt, M.P., Dyck, R.H., Simon, H.H., 2006. Slow progressive degeneration of nigral dopaminergic neurons in postnatal Engrailed mutant mice. Proc. Natl. Acad. Sci. USA 103, 15242–15247. https://doi.org/10.1073/pnas.0602116103.

Simon, H.H., Saueressig, H., Wurst, W., Goulding, M.D., O'Leary, D.D., 2001. Fate of midbrain dopaminergic neurons controlled by the engrailed genes. J. Neurosci. 21, 3126–3134.

Sobu, Y., Wawro, P.S., Dhekne, H.S., Yeshaw, W.M., Pfeffer, S.R., 2021. Pathogenic LRRK2 regulates ciliation probability upstream of tau tubulin kinase 2 via Rab10 and RILPL1 proteins. In: Proceedings of the National Academy of Sciences of the United States of America, 118. https://doi.org/10.1073/pnas.2005894118.

Sonnier, L., Le Pen, G., Hartmann, A., Bizot, J.-C., Trovero, F., Krebs, M.-O., Prochiantz, A., 2007. Progressive Loss of Dopaminergic Neurons in the Ventral Midbrain of Adult Mice Heterozygote for Engrailed1. J. Neurosci. 27, 1063–1071. https://doi.org/10.1523/JNEUROSCI.4583-06.2007.

Stettler, O., Joshi, R.L., Wizenmann, A., Reingruber, J., Holcman, D., Bouillot, C., Castagner, F., Prochiantz, A., Moya, K.L., 2012. Engrailed homeoprotein recruits the adenosine A1 receptor to potentiate ephrin A5 function in retinal growth cones. Development (Cambridge, England) 139, 215–224. https://doi.org/10.1242/dev.063875.

Stuermer, A., Hoehn, K., Faul, T., Auth, T., Brand, N., Kneissl, M., Pütter, V., Grummt, F., 2007. Mouse pre-replicative complex proteins colocalise and interact with the centrosome. Eur. J. Cell Biol. 86, 37–50. https://doi.org/10.1016/j.ejcb.2006.09.002.

Subramaniam, S.R., Chesselet, M.-F., 2013. Mitochondrial dysfunction and oxidative stress in Parkinson's disease. Prog. Neurobiol. 106-107, 17–32. https://doi.org/10.1016/j.pneurobio.2013.04.004.

Surmeier, D.J., Obeso, J.A., Halliday, G.M., 2017. Selective neuronal vulnerability in Parkinson disease. Nature reviews. Neuroscience 18, 101–113. https://doi.org/10.1038/nrn.2016.178.

Thomasson, N., Pioli, E., Friedel, C., Monseur, A., Lavaur, J., Moya, K.L., Bezard, E., Bousseau, A., Prochiantz, A., 2019. Engrailed-1 induces long-lasting behavior benefit in an experimental Parkinson primate model. Movem. Disord. : Off. J. Movem. Disord. Soc. 34, 1082–1084. https://doi.org/10.1002/mds.27714.

Tingler, M., Philipp, M., Burkhalter, M.D., 2022. DNA Replication proteins in primary microcephaly syndromes. Biol. Cell. 114, 143–159. https://doi.org/10.1111/boc.202100061.

Trcek, T., Sato, H., Singer, R.H., Maquat, L.E., 2013. Temporal and spatial characterization of nonsense-mediated mRNA decay. Gene Develop. 27, 541–551. https://doi.org/10.1101/gad.209635.112.

Volpato, V., Webber, C., 2020. Addressing variability in iPSC-derived models of human disease: guidelines to promote reproducibility. Dis. Model. Mech. 13 https://doi.org/10.1242/dmm.042317.

Vuolo, L., Stevenson, N.L., Mukhopadhyay, A.G., Roberts, A.J., Stephens, D.J., 2020. Cytoplasmic dynein-2 at a glance. J. Cell Sci. 133 https://doi.org/10.1242/jcs.240614.

Wang, Y., Chandran, J.S., Cai, H., Mattson, M.P., 2008. DJ-1 is essential for long-term depression at hippocampal CA1 synapses. NeuroMolecular Med. 10, 40–45. https://doi.org/10.1007/s12017-008-8023-4.

Wang, X., Sterr, M., Burtscher, I., Chen, S., Hieronimus, A., Machicao, F., Staiger, H., Häring, H.-U., Lederer, G., Meitinger, T., Cernilogar, F.M., Schotta, G., Irmler, M., Beckers, J., Hrabě de Angelis, M., Ray, M., Wright, C.V.E., Bakhti, M., Lickert, H., 2018. Genome-wide analysis of PDX1 target genes in human pancreatic progenitors. Mole. Metabol. 9, 57–68. https://doi.org/10.1016/j.molmet.2018.01.011.

Wang, Q., Zhang, Y., Wang, M., Song, W.-M., Shen, Q., McKenzie, A., Choi, I., Zhou, X., Pan, P.-Y., Yue, Z., Zhang, B., 2019. The landscape of multiscale transcriptomic networks and key regulators in Parkinson's disease. Nat. Commun. 10, 5234. https://doi.org/10.1038/s41467-019-13144-y.

Wheway, G., Nazlamova, L., Hancock, J.T., 2018. Signaling through the Primary Cilium. Fron. Cell Developm. Biol. 6, 8. https://doi.org/10.3389/fcell.2018.00008.

Wizenmann, A., Brunet, I., Lam, J., Sonnier, L., Beurdeley, M., Zarbalis, K., Weisenhorn-Vogt, D., Weinl, C., Dwivedy, A., Joliot, A., Wurst, W., Holt, C., Prochiantz, A., 2009. Extracellular Engrailed participates in the topographic guidance of retinal axons in vivo. Neuron 64, 355–366. https://doi.org/10.1016/j.neuron.2009.09.018.

Wurst, W., Auerbach, A.B., Joyner, A.L., 1994. Multiple developmental defects in Engrailed-1 mutant mice: an early mid-hindbrain deletion and patterning defects in forelimbs and sternum. Development (Cambridge, England) 120, 2065–2075. https://doi.org/10.1242/dev.120.7.2065.

Zhang, J., Götz, S., Vogt Weisenhorn, D.M., Simeone, A., Wurst, W., Prakash, N., 2015. A WNT1-regulated developmental gene cascade prevents dopaminergic neurodegeneration in adult En1(+/-) mice. Neurobiol. Dis. 82, 32–45. https://doi.org/10.1016/j.nbd.2015.05.015.